Extracting foreground-obscured μ-type distortion anisotropies with future CMB satellites

Mathieu Remazeilles

The University of Manchester

Remazeilles & Chluba
MNRAS 478, 807 (2018)

15th Marcel Grossmann Meeting
Rome, 1-7 July 2018

μ-type CMB spectral distortions

Sunyaev & Zeldovich 1970

- At pre-recombination era $(10^4 < z < 2 \times 10^6)$, energy injections into primordial plasma prevent *brehmsstrahlung* and *double Compton scattering* to create photons to maintain Planck's equilibrium, leading to Bose-Einstein (BE) equilibrium:

$$\boldsymbol{n_{BE} = n_{Pl} + \mu \underbrace{\frac{e^x}{(e^x - 1)^2}\left(\frac{x}{2.19} - 1\right)}_{}} \qquad x \equiv h\nu / kT_{CMB}$$

spectral signature of μ-distortion

- Caused by exciting physical processes at redshifts $z > 10^4$:
  - ✓ *Dissipation of primordial small-scale acoustic modes* – *Silk 1968*
  - ✓ *Annihilation / decay of relic particles* – *Hu & Silk 1993*
  - ✓ *Evaporation of primordial black holes* – *Carr et al 2010*
  - ✓ *Inflation with non-Bunch-Davies vacuum* – *Ganc & Komatsu 2012*

- LCDM: $|\mu| = 2.3 \times 10^{-8}$ – *Chluba 2016*
- COBE/FIRAS: $|\mu| < 9 \times 10^{-5}$ – *Fixsen et al 1996*

Spectral signature of distortions

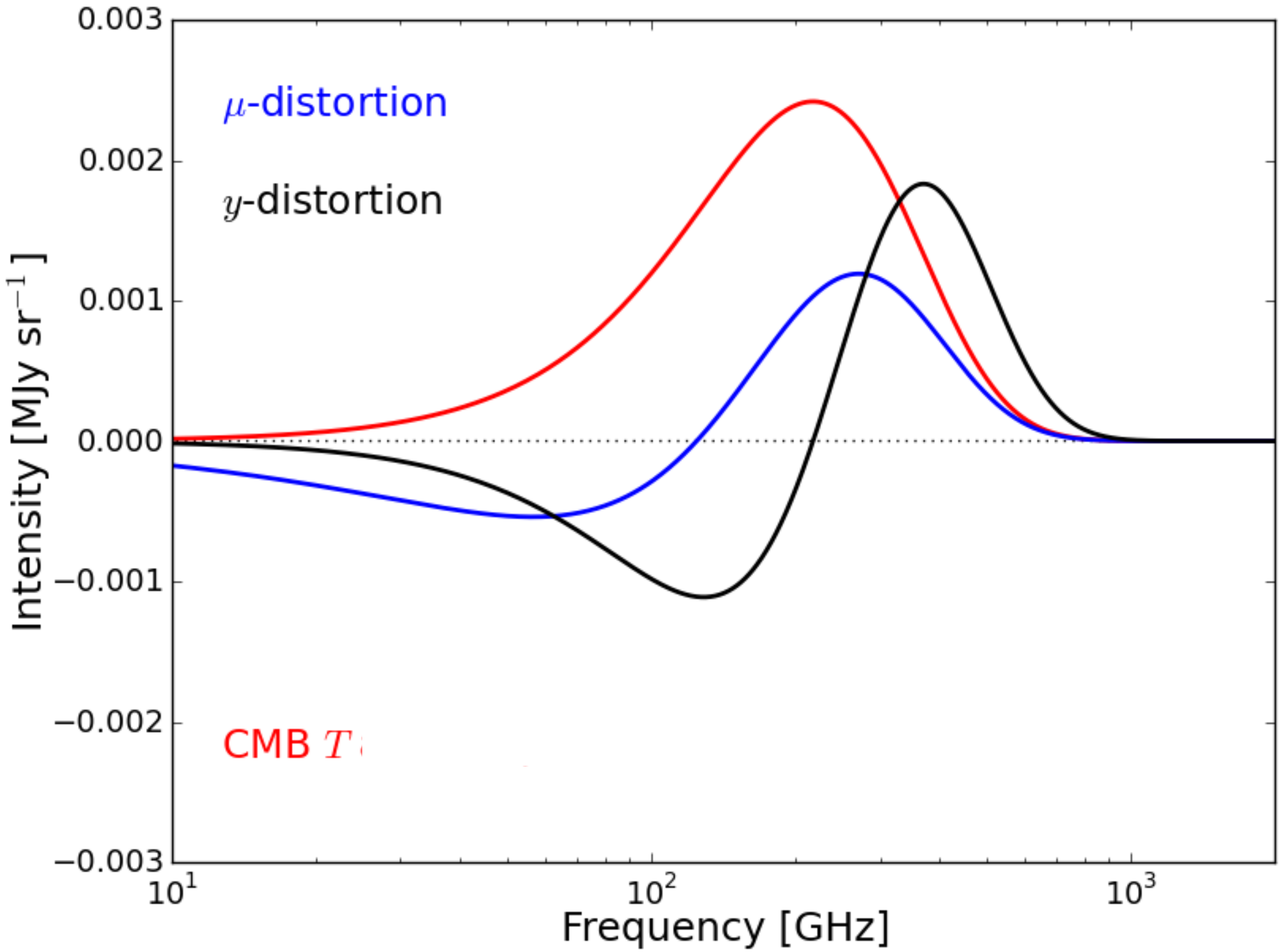

Distinct spectral signatures!

→ Multi-frequency observations allow to disentangle those signals

Anisotropic μ-type distortions

Aside from average CMB monopole distortions:

- Anisotropies of μ-type distortions (spectral-spatial anisotropies)

$$C_\ell^{\mu\mu} = 144 C_\ell^{TT,SW} f_{NL}^2 \langle \mu \rangle^2$$

- Correlation between CMB temperature and μ-type distortion anisotropies:

$$C_\ell^{\mu \times T} = 12 C_\ell^{TT,SW} \rho(\ell) f_{NL} \langle \mu \rangle$$

- Sources:
  - ✓ *Inflation with non-Bunch-davies initial state* *– Ganc & Komatsu 2012*
  - ✓ *Damping of primordial small-scale acoustic modes in the presence of enhanced primordial non-Gaussianity in the ultra-squeezed limit* *Pajer & Zaldarriaga 2012*

N.B.: Scale-dependent non-Gaussianity $f_{NL}(k) = f_{NL}(k_0)\left(\frac{k}{k_0}\right)^{n_{NL}-1}$ with $n_{NL} \simeq 1.6$

allows for: $\begin{cases} f_{NL}(k \simeq 740\ Mpc^{-1}) \simeq 4500 & (\mu\text{-distortion probe}) \\ f_{NL}(k_0 = 0.05\ Mpc^{-1}) \simeq 5 & (\text{CMB probe}) \end{cases}$

μ-type distortion anisotropies

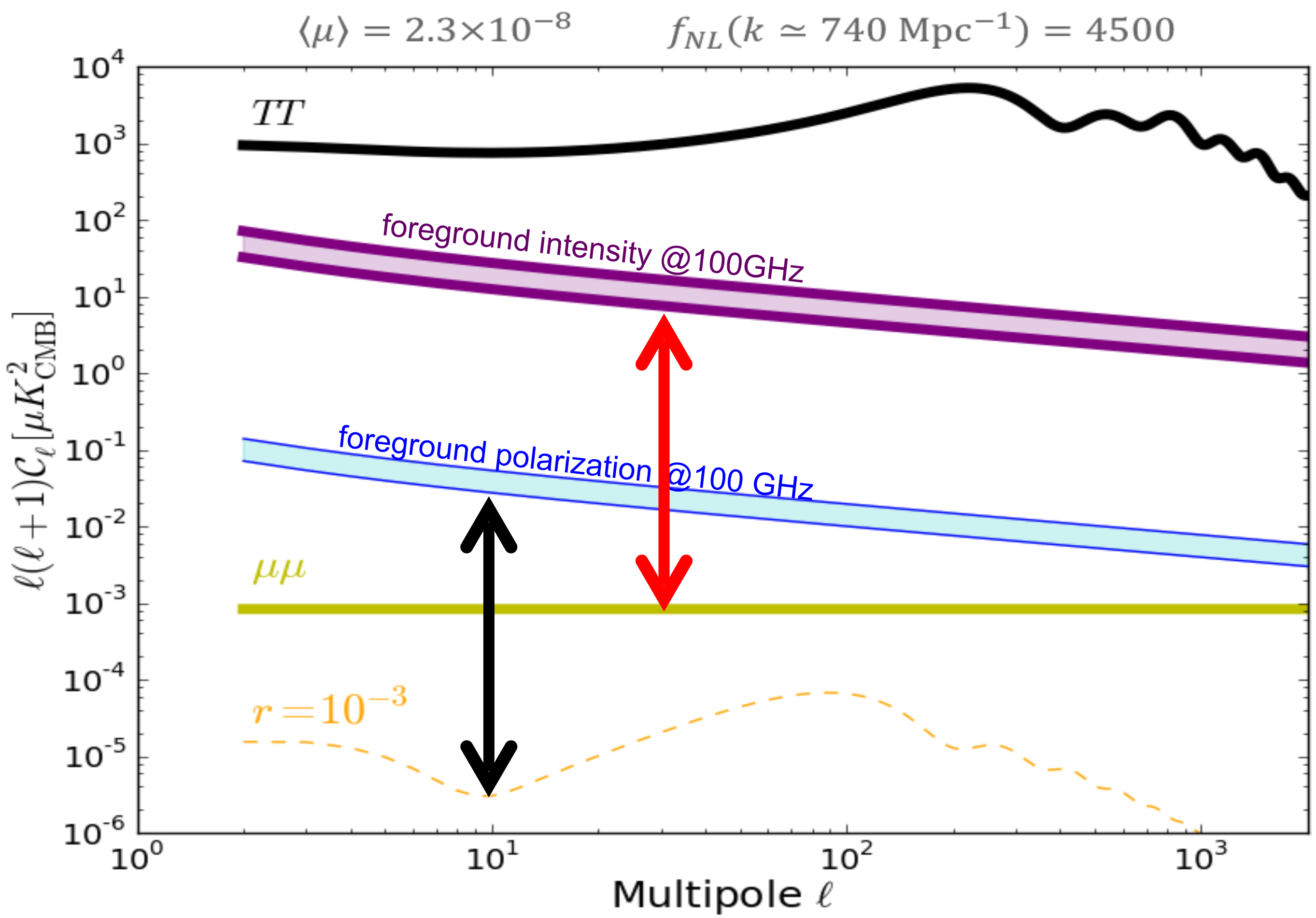

Same dynamic range (signal-to-foregrounds ratio) than for B-modes at $r = 10^{-3}$

$\rightarrow$ ***A science case for future CMB satellites!***

μ-type distortion anisotropies

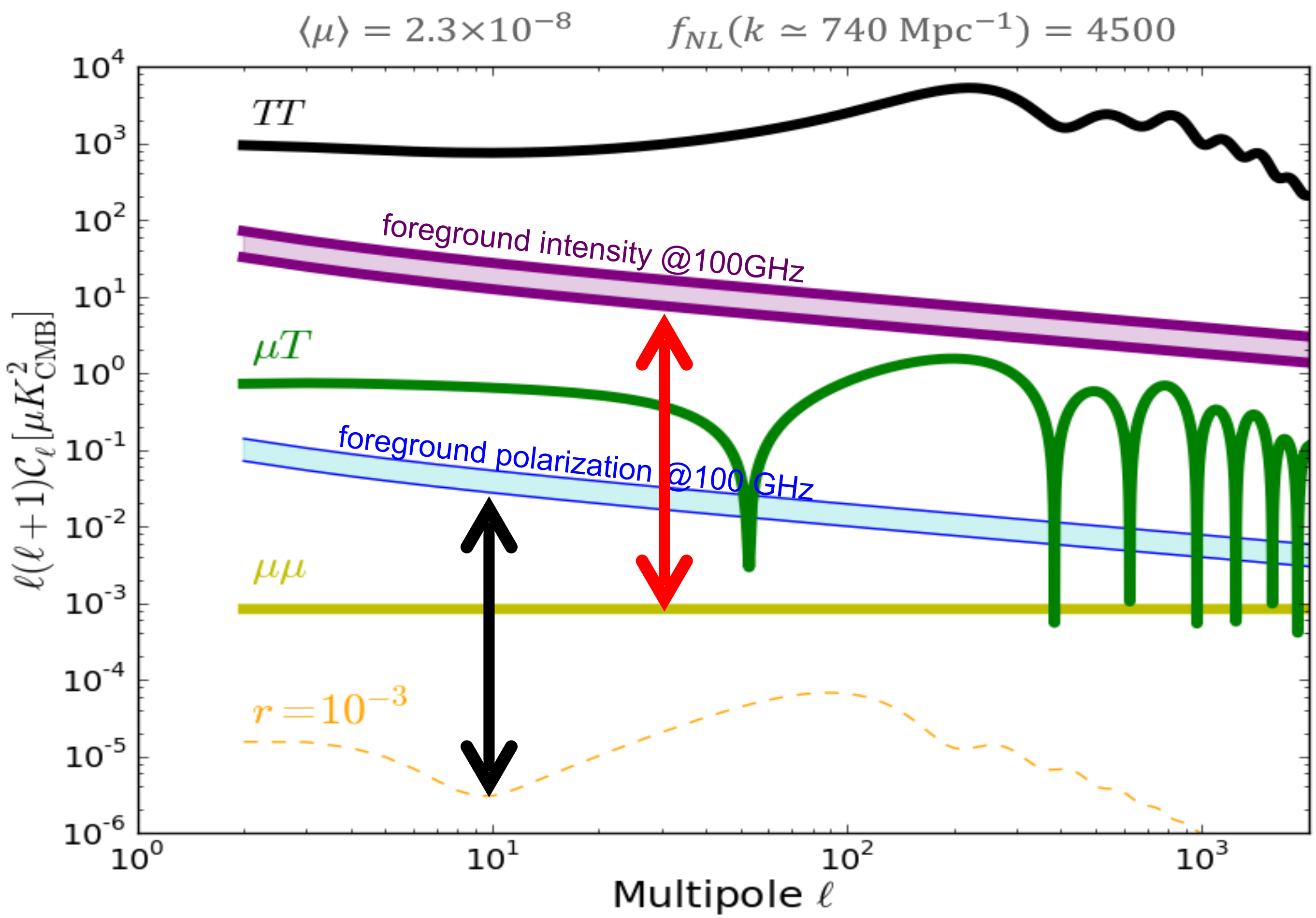

μ-T cross-power spectrum:

Enhanced μ-type distortion signal through correlation with CMB temperature anisotropies!

→ ***Accessible signal for future CMB satellites!***

Questions

- *Can we detect the μ-T correlated signal with future CMB satellites?*

- *What constraints on $f_{NL}(k \simeq 740\ \mathrm{Mpc}^{-1})$ can be achieved in the presence of foregrounds?*

The problem of foregrounds

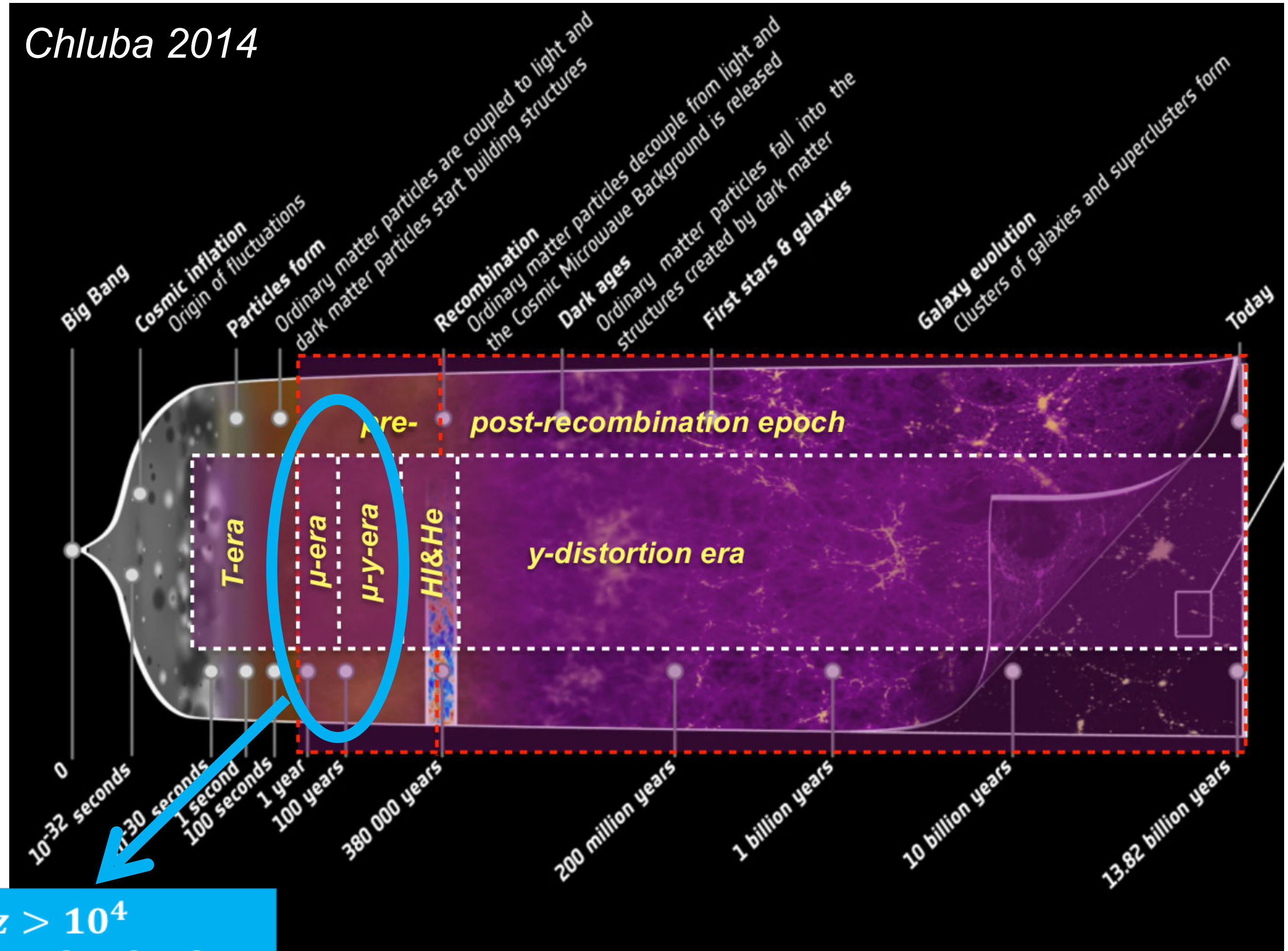

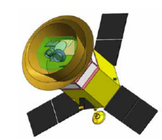

$z > 10^4$
cosmological
μ-distortion signal

$z = 0$
Galactic
foregrounds

μ-type spectral distortions open a new window to probe physics occurring behind the last-scattering surface, where the universe is invisible!

The problem of foregrounds

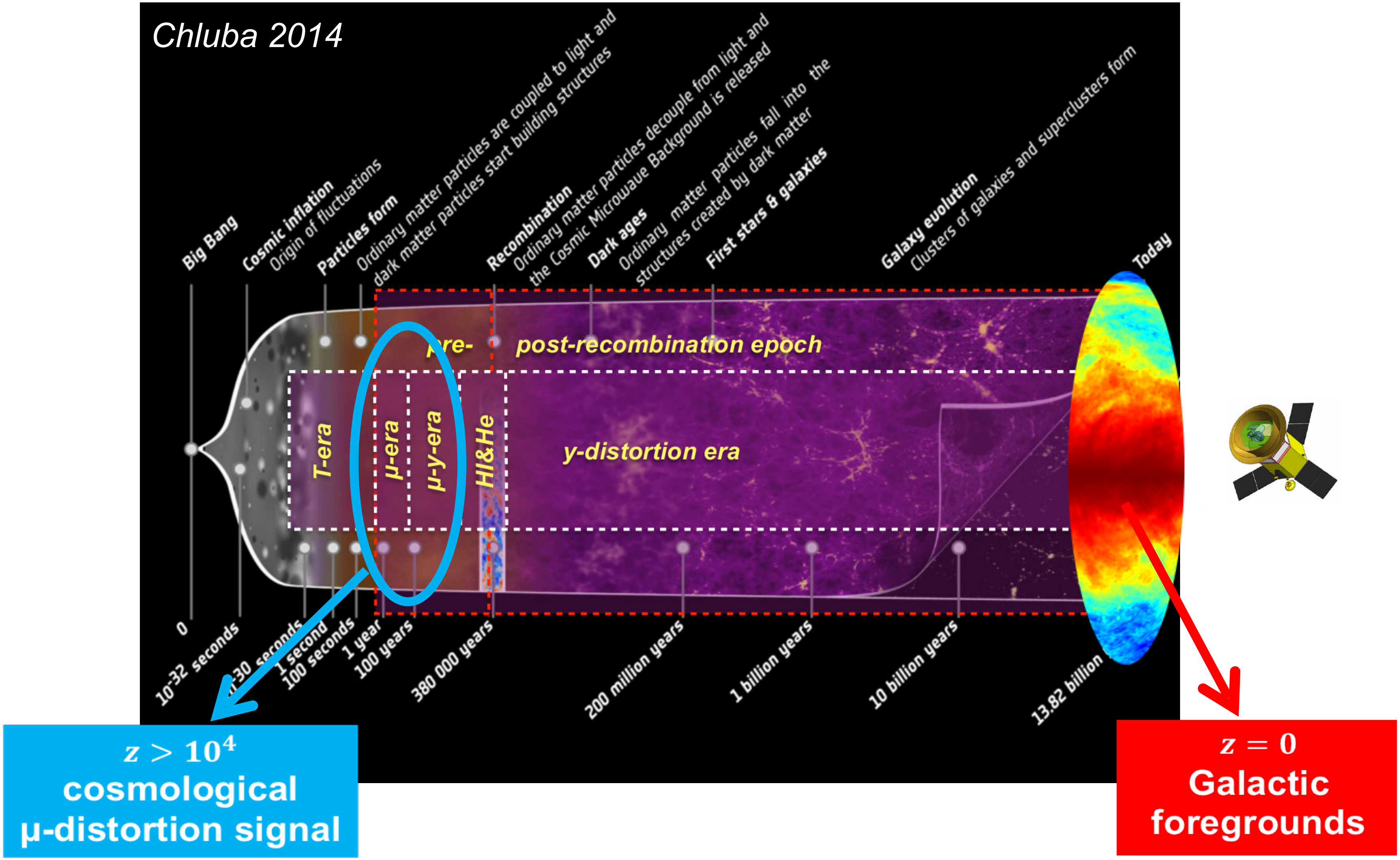

μ-type spectral distortions open a new window to probe physics occurring behind the last-scattering surface, where the universe is invisible!

The problem of foregrounds

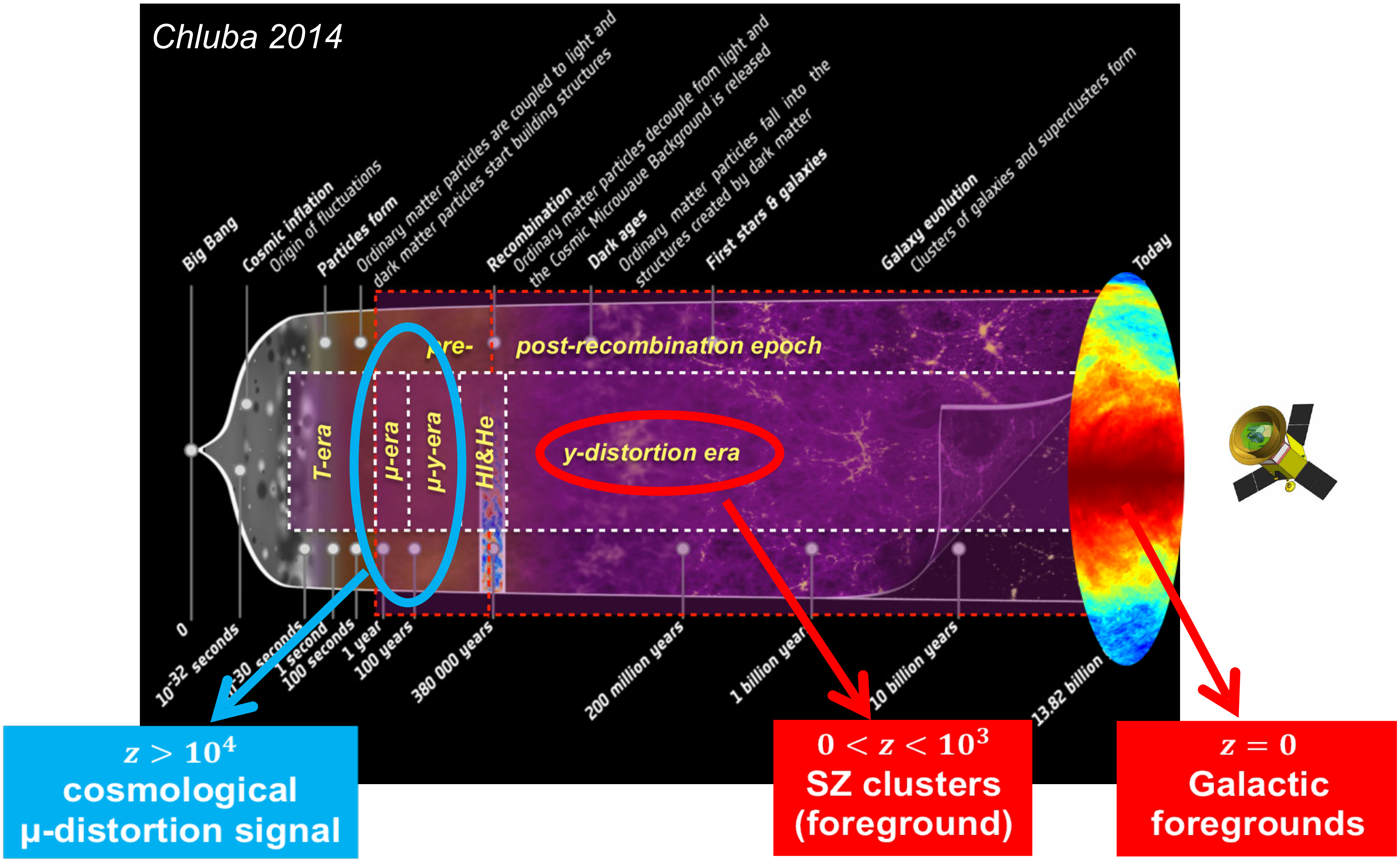

μ-type spectral distortions open a new window to probe physics occurring behind the last-scattering surface, where the universe is invisible!

The problem of foregrounds

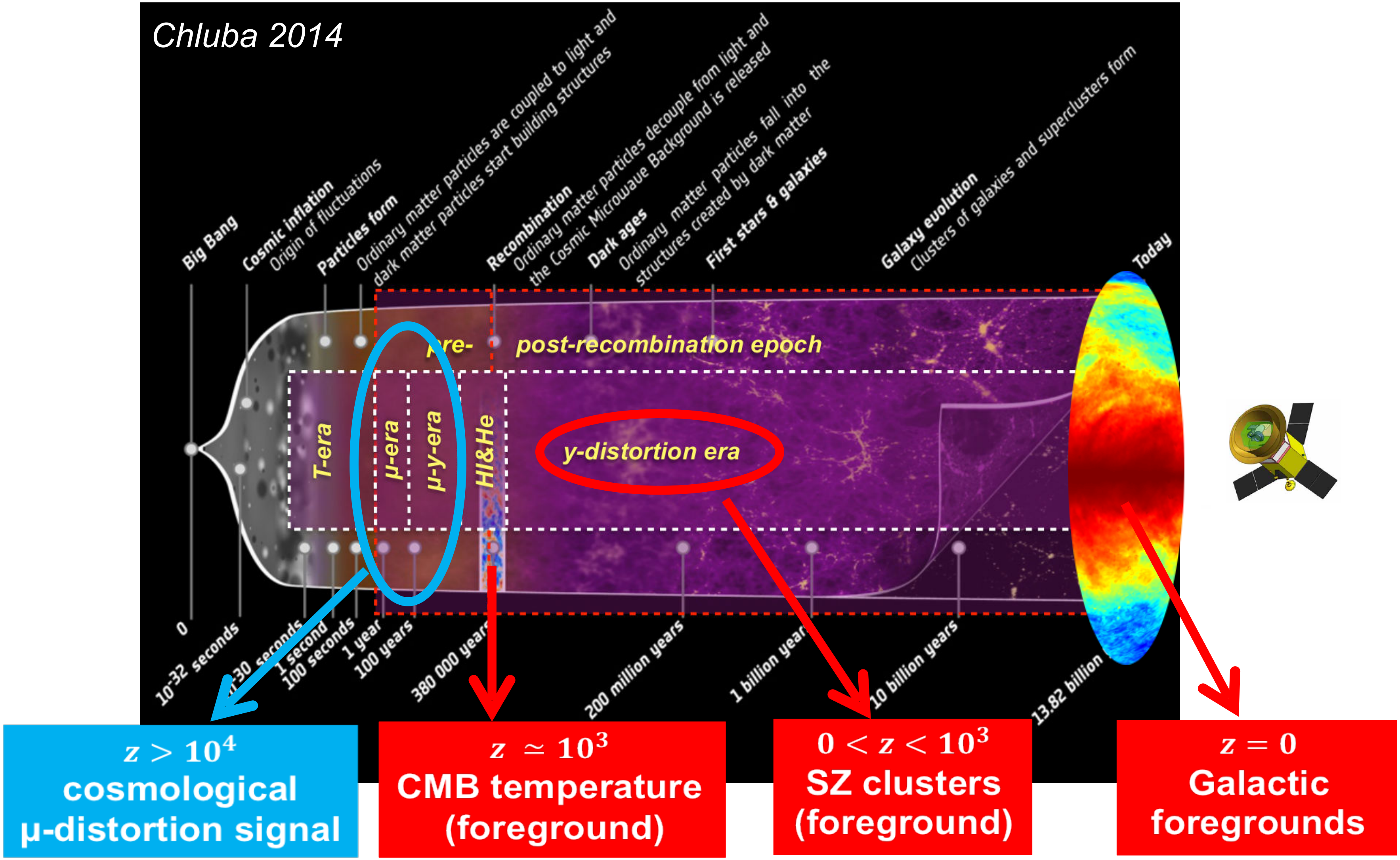

μ-type spectral distortions open a new window to probe physics occurring behind the last-scattering surface, where the universe is invisible!

Component separation : the problem

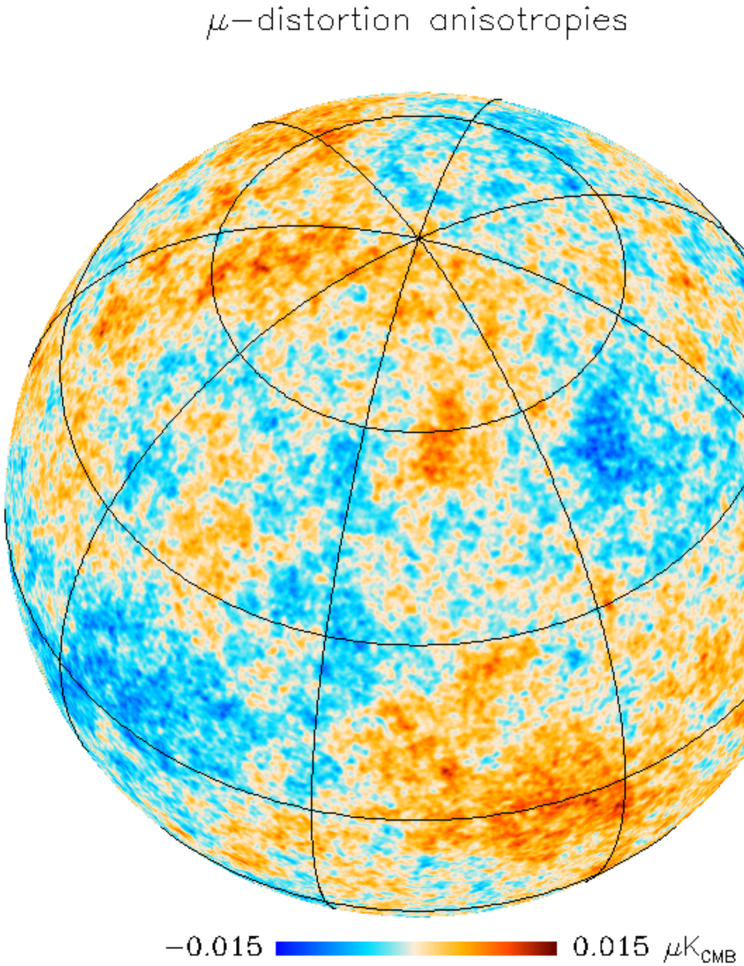

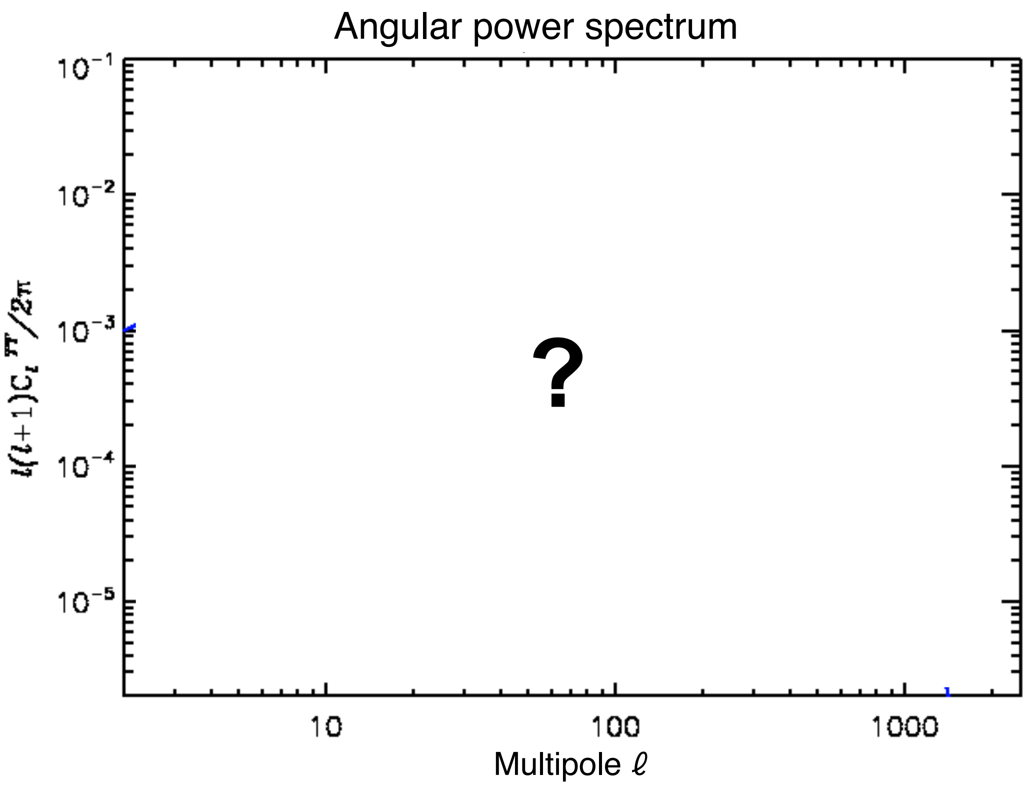

Component separation : the problem

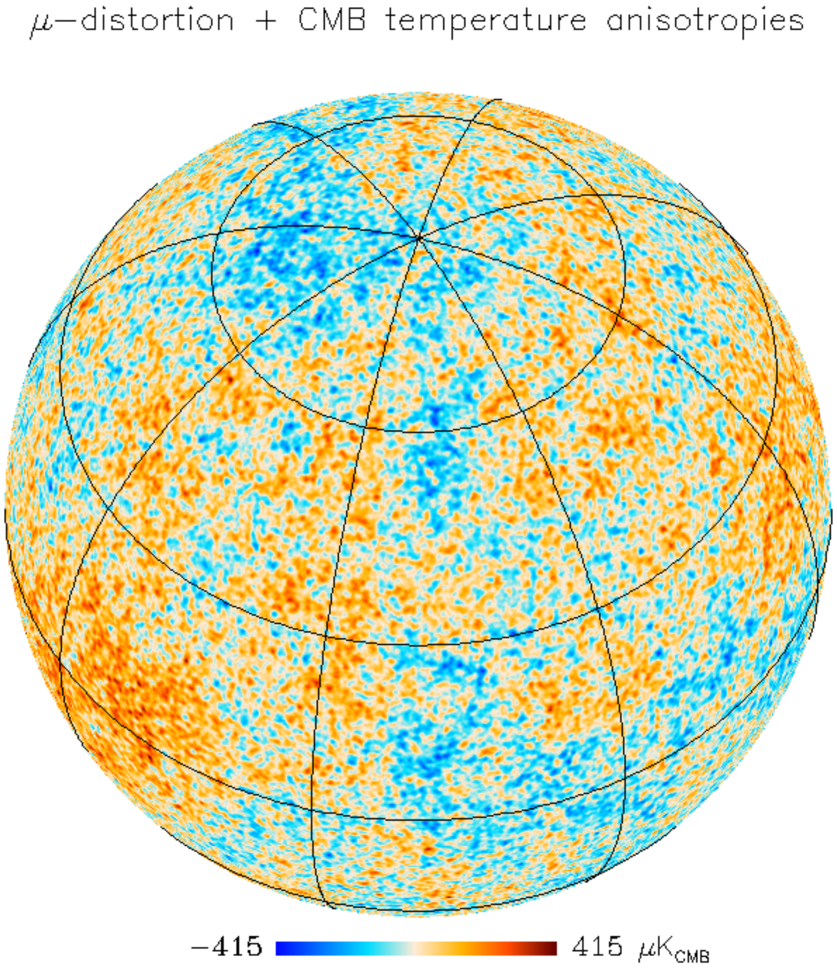

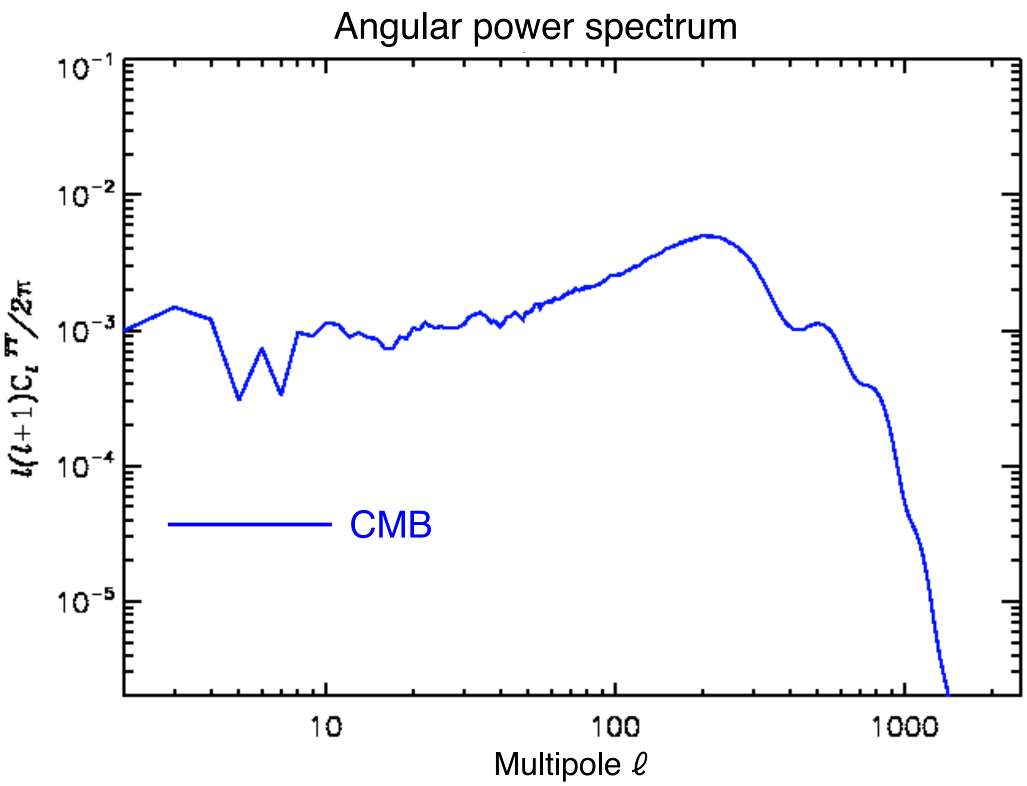

Component separation : the problem

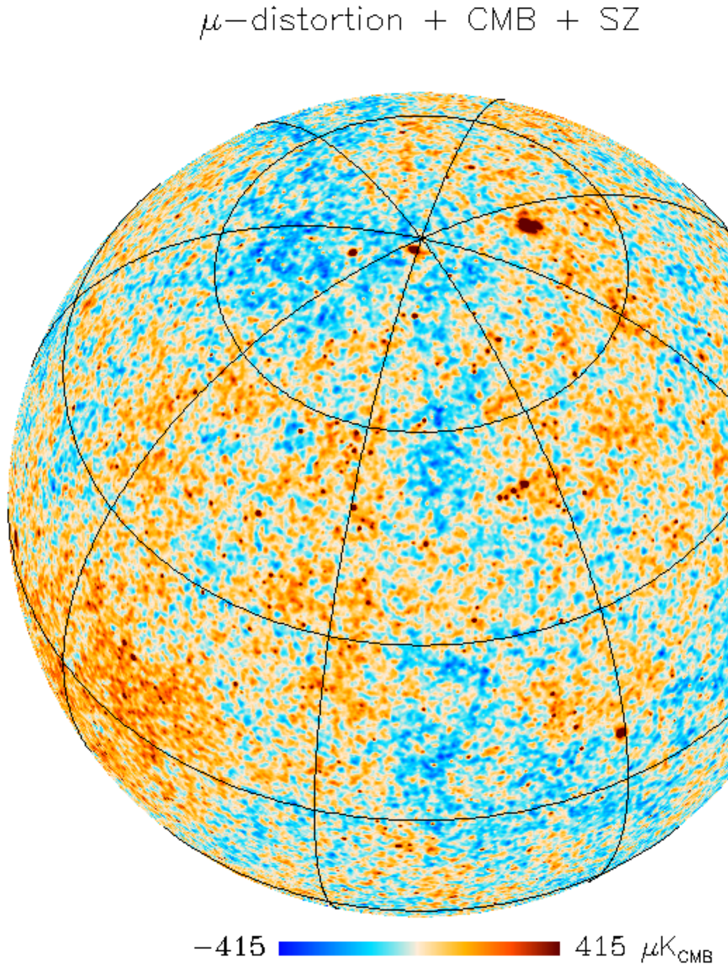

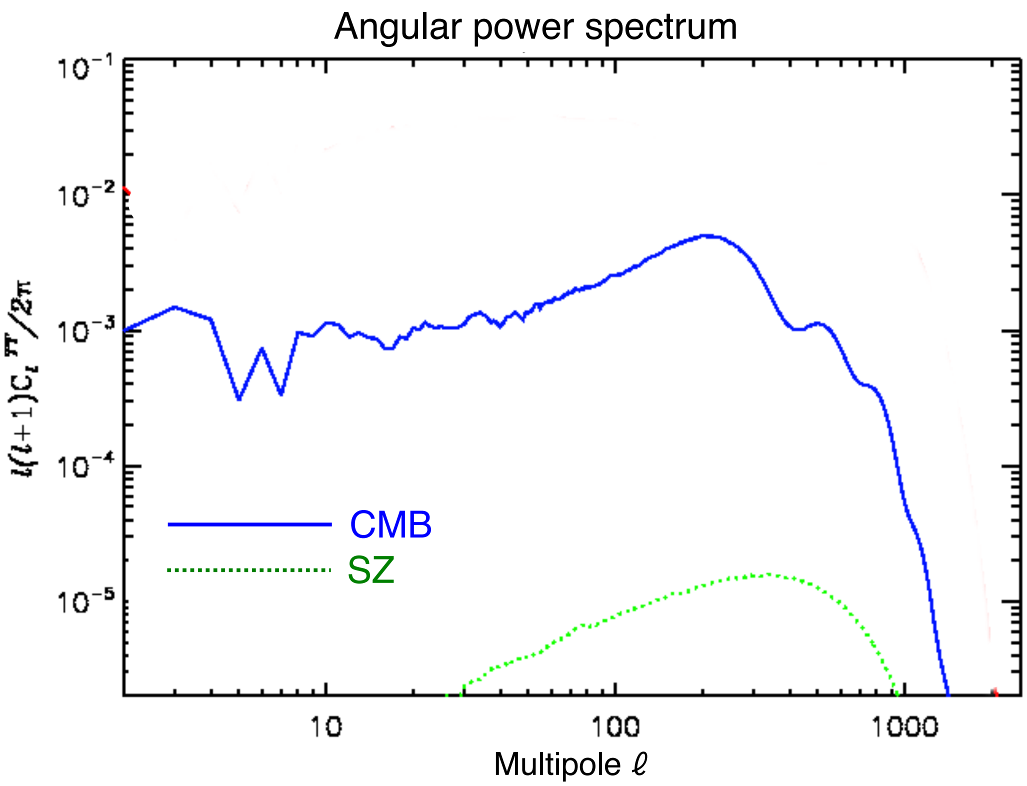

Component separation : the problem

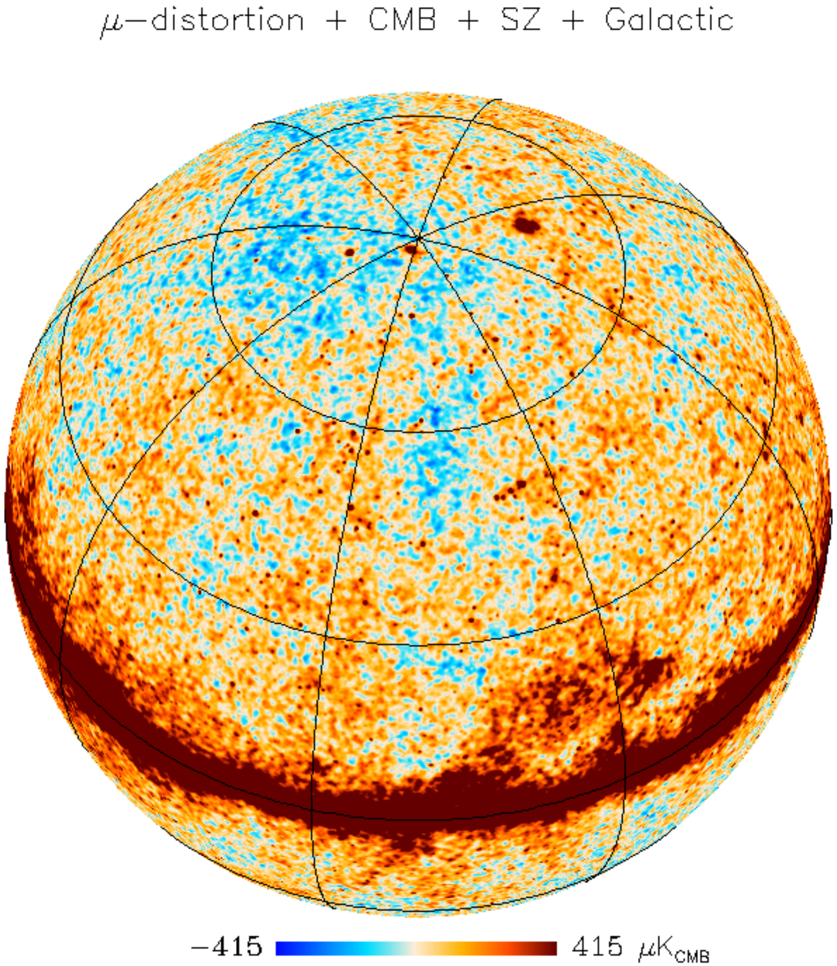

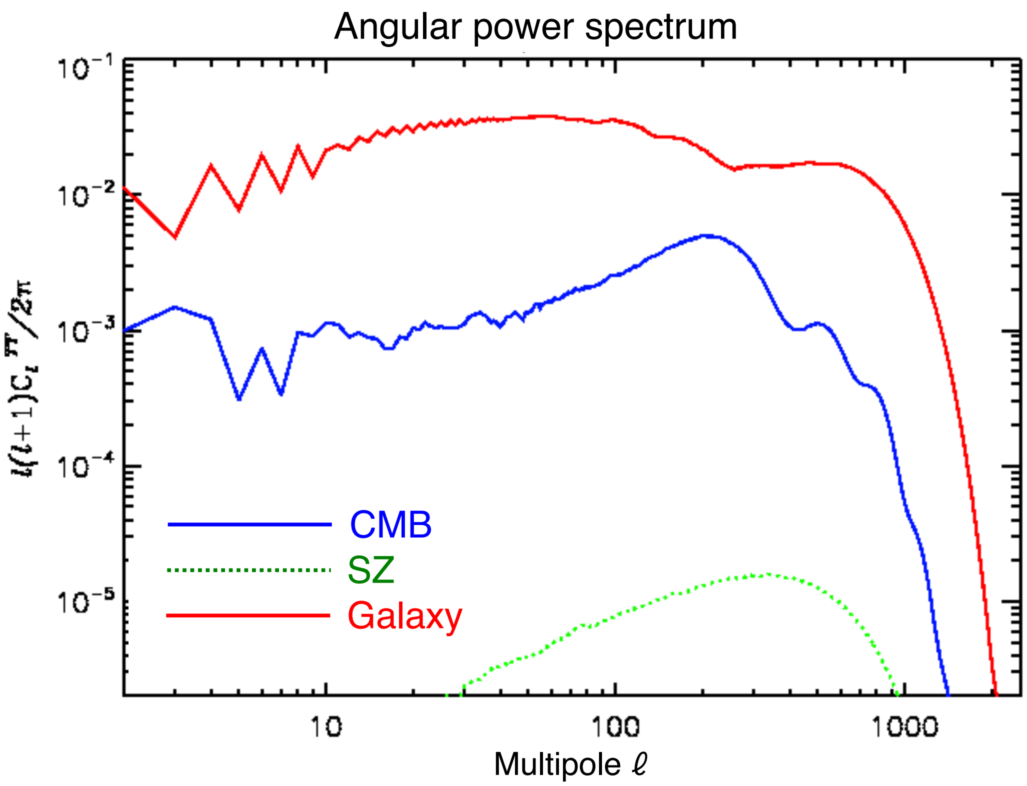

Component separation : the problem

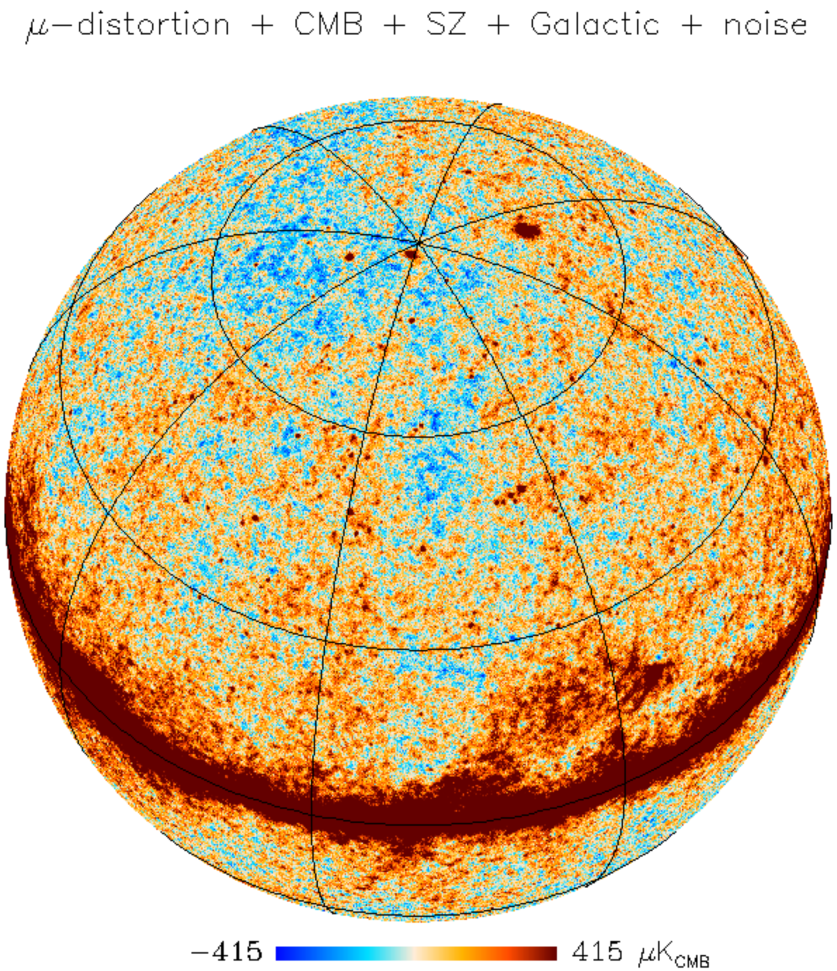

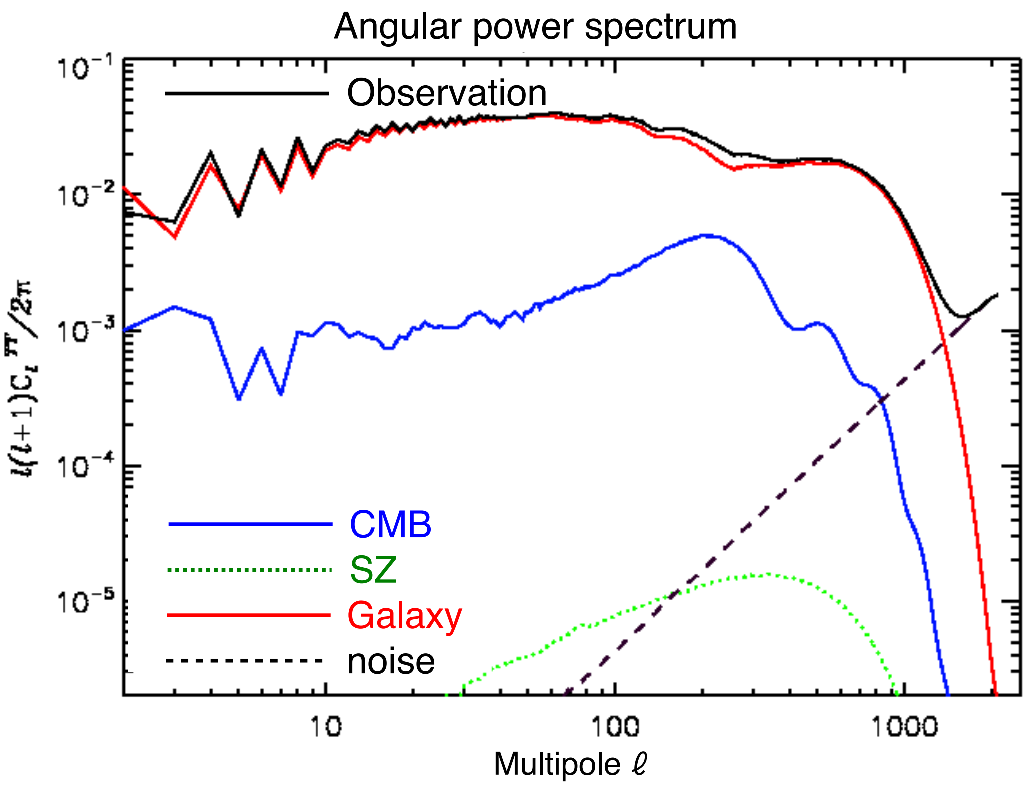

The problem of the CMB temp. foreground

$$\boldsymbol{d}(\boldsymbol{\nu},\underline{\boldsymbol{\theta}}) = \boldsymbol{a}(\boldsymbol{\nu})\,\boldsymbol{\mu}(\underline{\boldsymbol{\theta}}) + \boldsymbol{b}(\boldsymbol{\nu})\,\boldsymbol{T}(\underline{\boldsymbol{\theta}}) + Galactic\ foregrounds + noise$$

sky observation at frequency ν and direction $\underline{\theta}$

μ-distortion anisotropies

CMB temperature anisotropies

- CMB T anisotropies: a major foreground to μ-type distortion anisotropies

- CMB T anisotropies: a foreground that is <u>correlated</u> to the μ-anisotropy signal!

→ *This might be an issue for component separation*

Component separation: standard ILC

$$\boldsymbol{d}(\boldsymbol{\nu},\underline{\boldsymbol{\theta}}) = \boldsymbol{a}(\boldsymbol{\nu})\,\boldsymbol{\mu}(\underline{\boldsymbol{\theta}}) + \boldsymbol{b}(\boldsymbol{\nu})\,\boldsymbol{T}(\underline{\boldsymbol{\theta}}) + Galactic\ foregrounds + noise$$

- Weighted linear combination of frequency maps:

$$\widehat{\boldsymbol{\mu}}(\underline{\boldsymbol{\theta}}) = \sum_{\boldsymbol{\nu}} \boldsymbol{w}(\boldsymbol{\nu})\,\boldsymbol{d}(\boldsymbol{\nu},\underline{\boldsymbol{\theta}}) \quad \text{such that} \quad \begin{cases} \boldsymbol{w}^{\boldsymbol{t}}\langle \boldsymbol{d}\boldsymbol{d}^{\boldsymbol{t}}\rangle \boldsymbol{w}\ \text{min. var.} \\ \sum_{\boldsymbol{\nu}} \boldsymbol{w}(\boldsymbol{\nu})\,\boldsymbol{a}(\boldsymbol{\nu}) = \mathbf{1} \end{cases}$$

- Analytic solution: $\boldsymbol{w}^{\boldsymbol{t}} = \dfrac{\boldsymbol{a}^{\boldsymbol{t}}\boldsymbol{C}^{-\mathbf{1}}}{\boldsymbol{a}^{\boldsymbol{t}}\boldsymbol{C}^{-\mathbf{1}}\boldsymbol{a}}$ $\quad (C \equiv \langle dd^t \rangle)$

Benett et al, 2003
Tegmark et al, 2003
Eriksen et al, 2004
Delabrouille et al, 2009

- Problem:

→ residual CMB T anisotropies in the ILC reconstructed μ-map

$$\widehat{\boldsymbol{\mu}}(\underline{\boldsymbol{\theta}}) = \boldsymbol{\mu}\,(\underline{\boldsymbol{\theta}}) + (\boldsymbol{w}^{\boldsymbol{t}}b)\,\boldsymbol{T}(\underline{\boldsymbol{\theta}}) + \ \ldots$$

→ residual TT correlations in the measured μ-T cross-power spectrum!

$$\langle \widehat{\boldsymbol{\mu}}(\underline{\boldsymbol{\theta}})\boldsymbol{T}(\underline{\boldsymbol{\theta}}')\rangle = \underbrace{\langle \boldsymbol{\mu}(\underline{\boldsymbol{\theta}})\boldsymbol{T}(\underline{\boldsymbol{\theta}}')\rangle}_{\text{signal}} + \boldsymbol{\varepsilon}\,\underbrace{\langle \boldsymbol{T}(\underline{\boldsymbol{\theta}})\boldsymbol{T}(\underline{\boldsymbol{\theta}}')\rangle}_{TT\ \text{residuals bury the signal!}} + \ \ldots$$

Component separation: Constrained-ILC

$$\boldsymbol{d}(\boldsymbol{\nu}, \underline{\boldsymbol{\theta}}) = \boldsymbol{a}(\boldsymbol{\nu})\, \boldsymbol{\mu}(\underline{\boldsymbol{\theta}}) + \boldsymbol{b}(\boldsymbol{\nu})\, \boldsymbol{T}(\underline{\boldsymbol{\theta}}) + Galactic\ foregrounds + noise$$

- Weighted linear combination of frequency maps:

$$\widehat{\boldsymbol{\mu}}(\underline{\boldsymbol{\theta}}) = \sum_{\boldsymbol{\nu}} \boldsymbol{w}(\boldsymbol{\nu})\, \boldsymbol{d}(\boldsymbol{\nu}, \underline{\boldsymbol{\theta}}) \quad \text{such that} \quad \begin{cases} \boldsymbol{w}^t \langle \boldsymbol{d}\boldsymbol{d}^t \rangle \boldsymbol{w} \ \text{min. var.} \\ \sum_{\boldsymbol{\nu}} \boldsymbol{w}(\boldsymbol{\nu})\, \boldsymbol{a}(\boldsymbol{\nu}) = \boldsymbol{1} \\ \sum_{\boldsymbol{\nu}} \boldsymbol{w}(\boldsymbol{\nu})\, \boldsymbol{b}(\boldsymbol{\nu}) = \boldsymbol{0} \end{cases}$$

→ *orthogonality to CMB T spectrum*

- Analytic solution: $\boldsymbol{w}^t = \dfrac{(\boldsymbol{b}^t\, \boldsymbol{C}^{-1} \boldsymbol{b})\boldsymbol{a}^t \boldsymbol{C}^{-1} - (\boldsymbol{a}^t \boldsymbol{C}^{-1} \boldsymbol{b})\boldsymbol{b}^t \boldsymbol{C}^{-1}}{(\boldsymbol{a}^t \boldsymbol{C}^{-1} \boldsymbol{a})(\boldsymbol{b}^t \boldsymbol{C}^{-1} \boldsymbol{b}) - (\boldsymbol{a}^t \boldsymbol{C}^{-1} \boldsymbol{b})^2}$

Remazeilles et al, 2011
Remazeilles & Chluba, 2018

→ No more residual CMB T anisotropies in the reconstructed μ-map

$$\widehat{\boldsymbol{\mu}}(\underline{\boldsymbol{\theta}}) = \boldsymbol{\mu}\,(\underline{\boldsymbol{\theta}}) + \underbrace{(\boldsymbol{w}^t \boldsymbol{b})}_{=0}\ \boldsymbol{T}(\underline{\boldsymbol{\theta}}) + \ \ldots$$

→ No more residual TT correlations in the μ-T cross-power spectrum!

$$\langle \widehat{\boldsymbol{\mu}}(\underline{\boldsymbol{\theta}}) \boldsymbol{T}(\underline{\boldsymbol{\theta}'}) \rangle = \langle \boldsymbol{\mu}(\underline{\boldsymbol{\theta}}) \boldsymbol{T}(\underline{\boldsymbol{\theta}'}) \rangle + \boldsymbol{\varepsilon}\, \cancel{\langle \boldsymbol{T}(\underline{\boldsymbol{\theta}}) \boldsymbol{T}(\underline{\boldsymbol{\theta}'}) \rangle} \ + \ \ldots$$

Standard ILC vs Constrained ILC

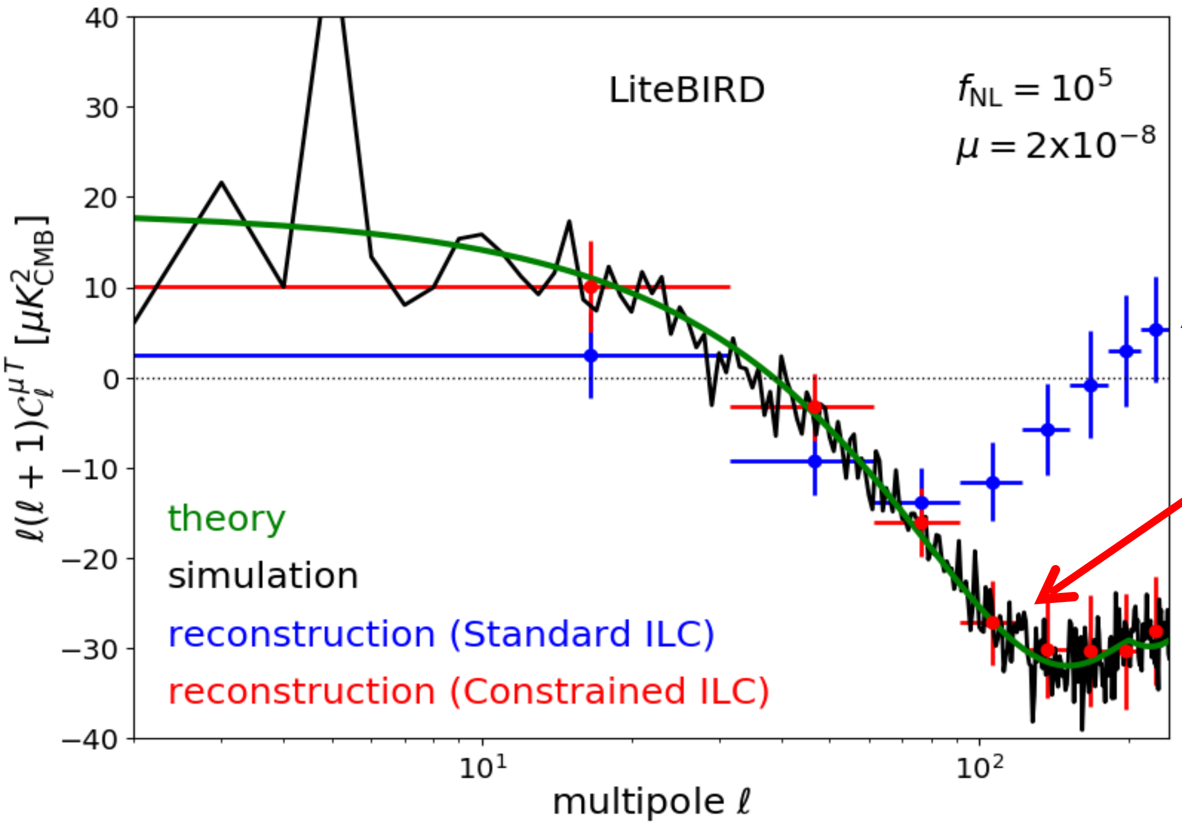

Standard ILC methods suffer from spurious TT correlations due to CMB residuals in the μ-map

The Constrained-ILC fully recovers the correlated μ-T signal without bias

In light of these considerations, the constraints on $C_\ell^{\mu T}$ from Planck data by Khatri & Sunyaev (2015) should be taken cautiously

Remazeilles & Chluba (2018)

The Constrained-ILC idea
can also be used to kill residual y-distortions
in CMB temperature map

Standard ILC

input thermal SZ

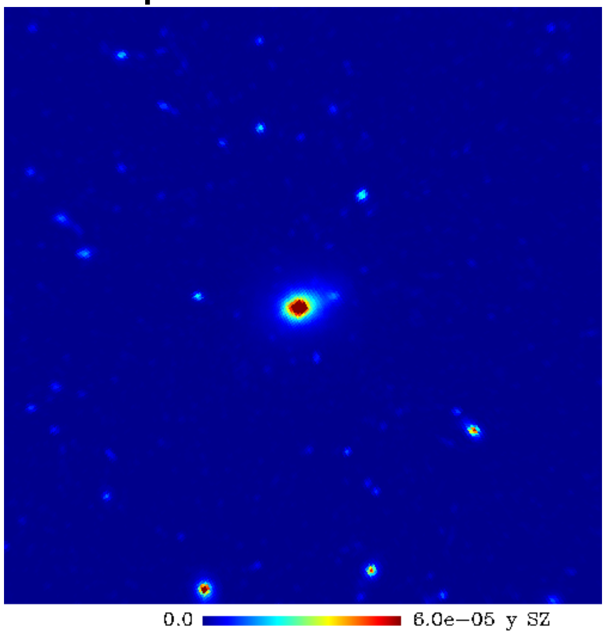

input kinetic SZ

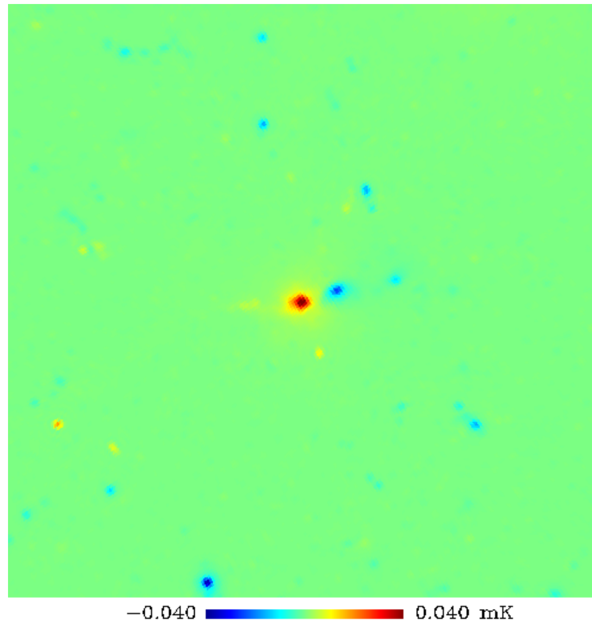

input CMB

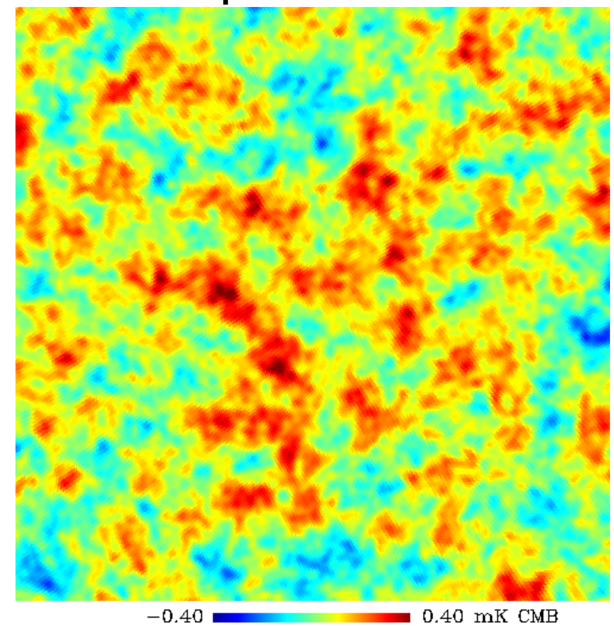

ILC

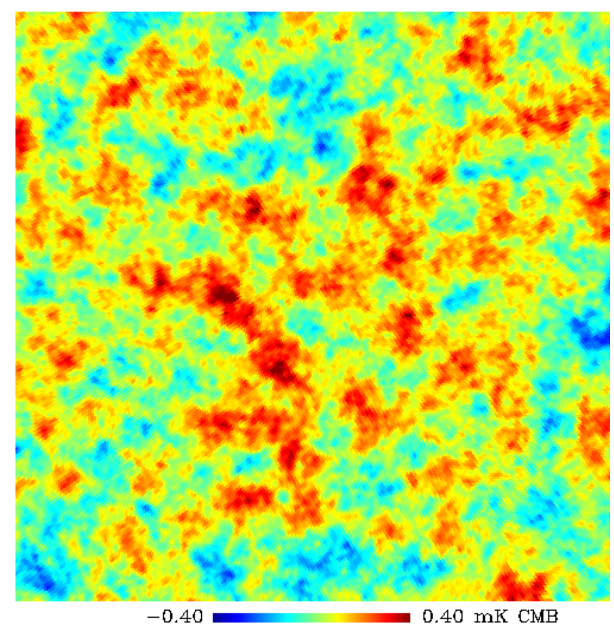

$$\boldsymbol{w^t = \frac{a^t C^{-1}}{a^t C^{-1} a}}$$

Bennett et al (2003), Tegmark et al (2003)
Eriksen et al (2004), Delabrouille et al (2009)

Standard ILC

input thermal SZ

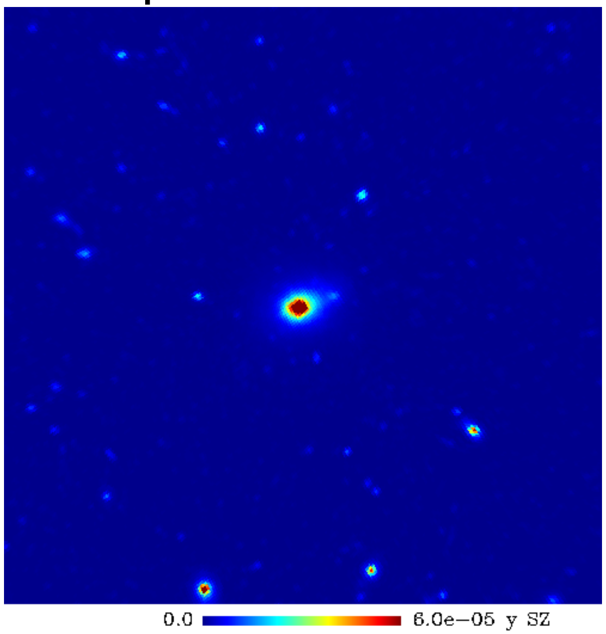

input kinetic SZ

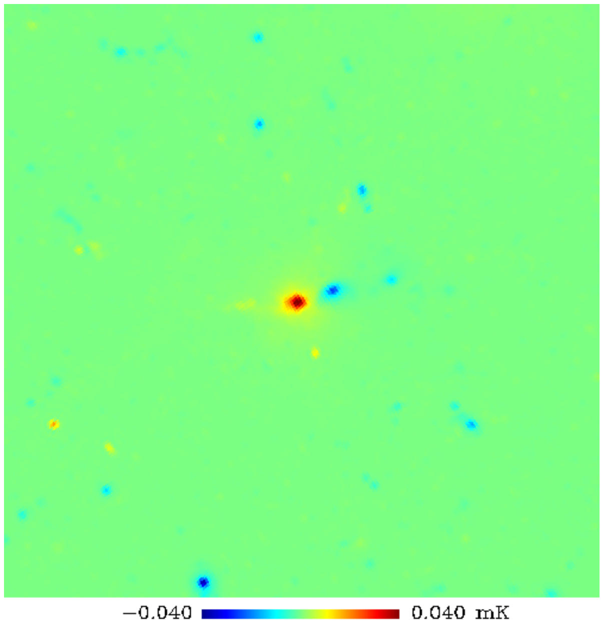

input CMB

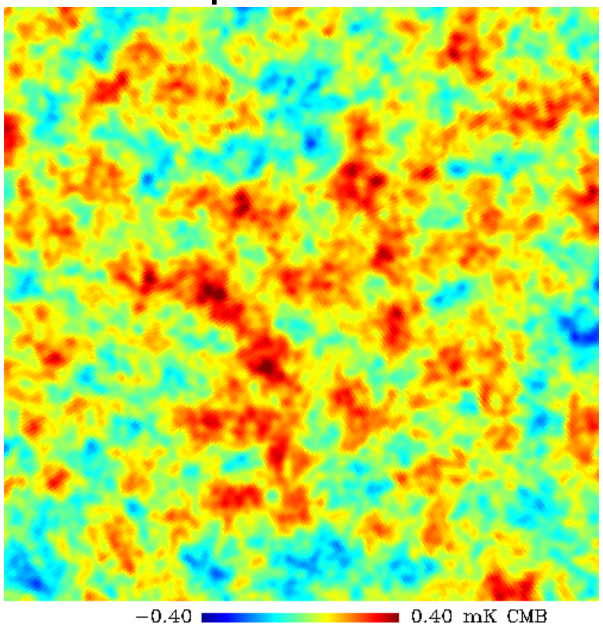

Thermal SZ / y-distortion residuals!
(clusters in the CMB)

error: ILC - CMB

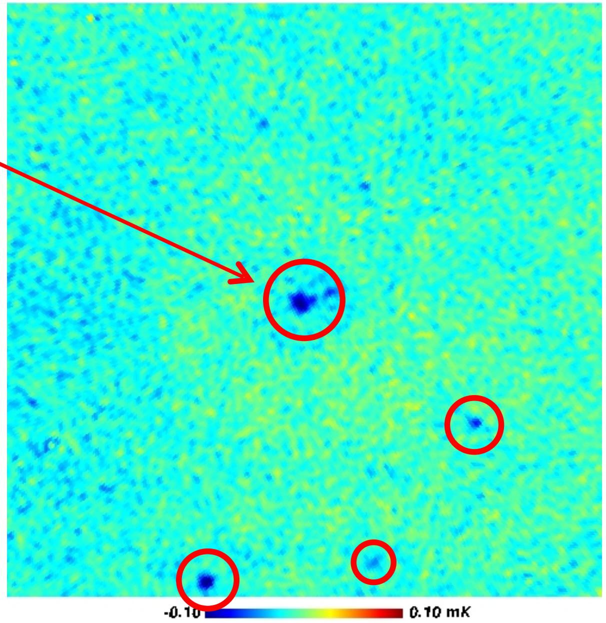

$$\boldsymbol{w}^t = \frac{\boldsymbol{a}^t\boldsymbol{C}^{-1}}{\boldsymbol{a}^t\boldsymbol{C}^{-1}\boldsymbol{a}}$$

Bennett et al (2003), Tegmark et al (2003)
Eriksen et al (2004), Delabrouille et al (2009)

Constrained-ILC

input thermal SZ

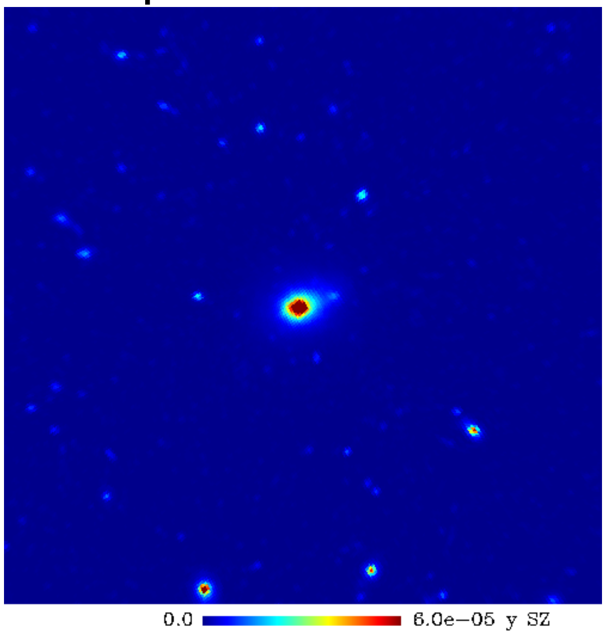

input kinetic SZ

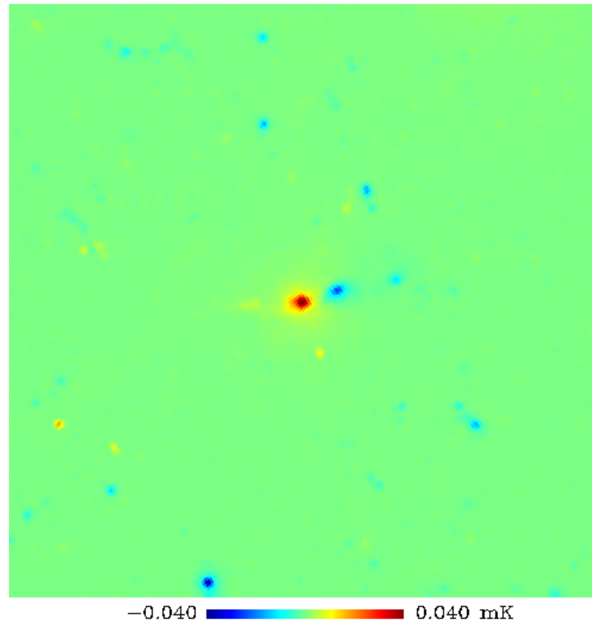

input CMB

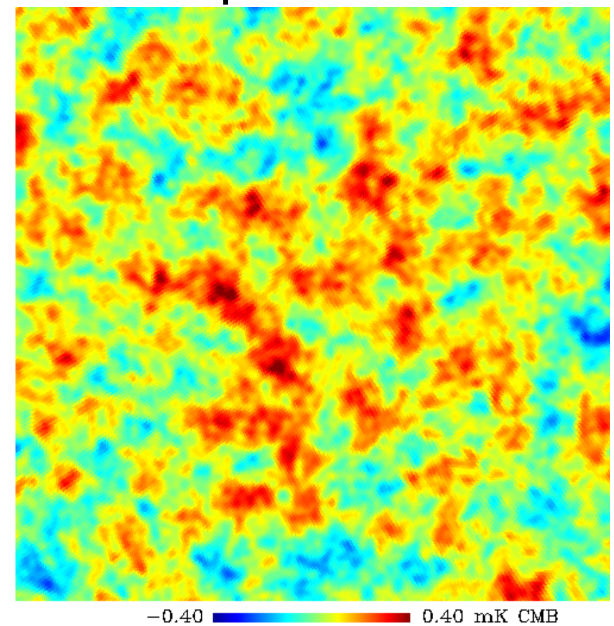

error: Constrained ILC - CMB

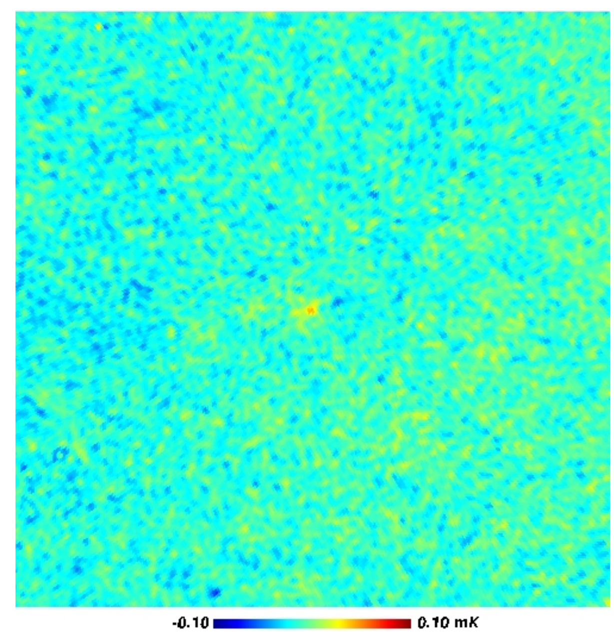

$$\boldsymbol{w}^t = \frac{(\boldsymbol{b}^t\boldsymbol{C}^{-1}\boldsymbol{b})\boldsymbol{a}^t\boldsymbol{C}^{-1} - (\boldsymbol{a}^t\boldsymbol{C}^{-1}\boldsymbol{b})\boldsymbol{b}^t\boldsymbol{C}^{-1}}{(\boldsymbol{a}^t\boldsymbol{C}^{-1}\boldsymbol{a})(\boldsymbol{b}^t\boldsymbol{C}^{-1}\boldsymbol{b}) - (\boldsymbol{a}^t\boldsymbol{C}^{-1}\boldsymbol{b})^2}$$

Remazeilles, Delabrouille, Cardoso, MNRAS (2011)

Forecasts on μ-distortion anisotropies
from
sky simulations of future CMB satellites

Simulation of correlated μ and T fields

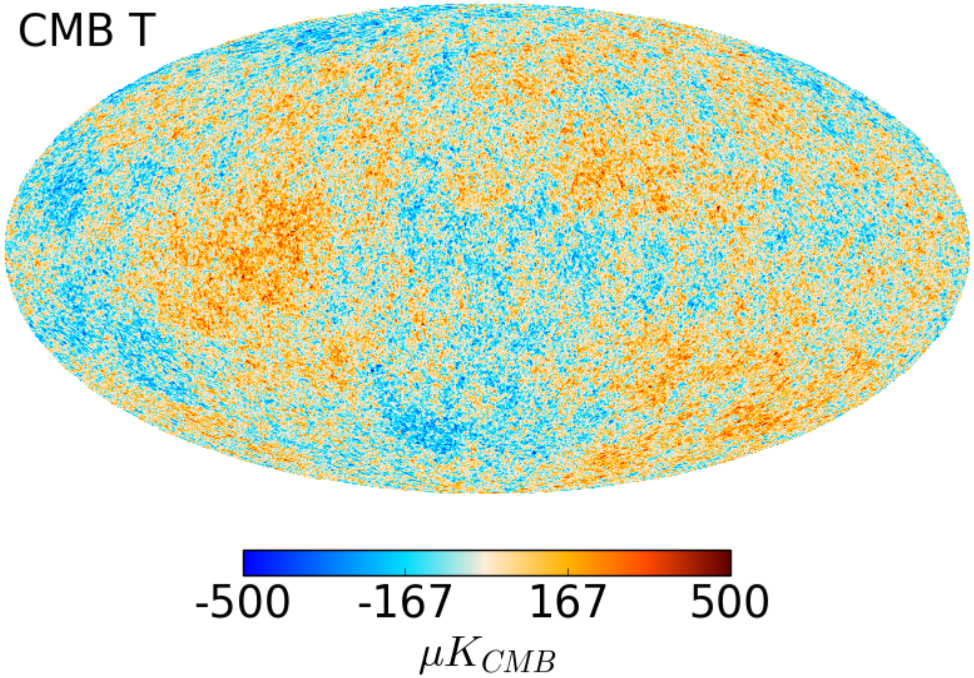

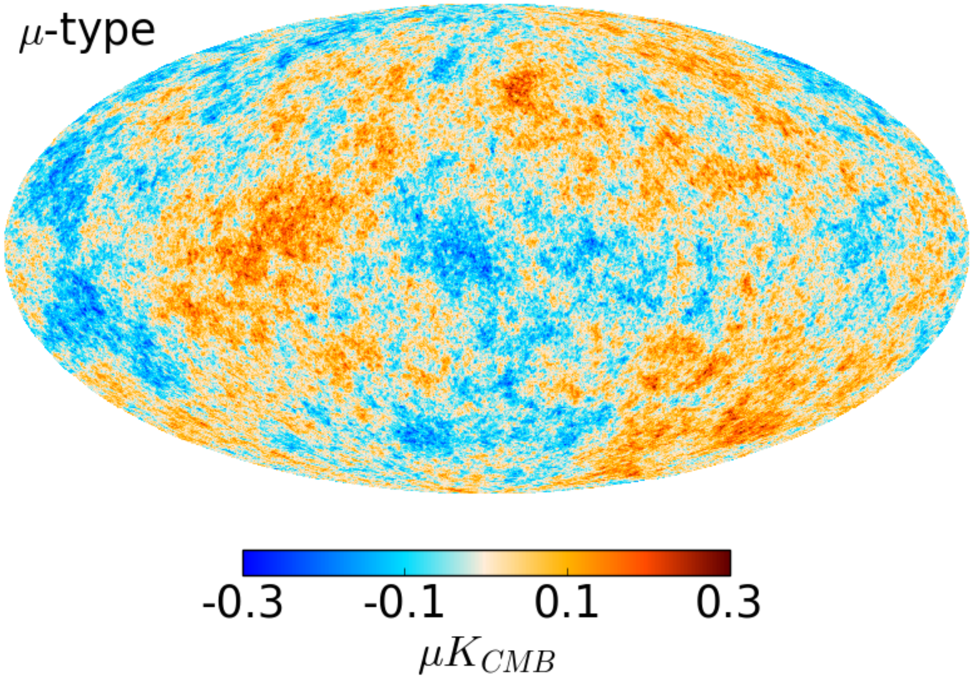

$\langle\mu\rangle = 2\times10^{-8}$ $\quad$ $f_{NL}(k \simeq 740\ \mathrm{Mpc}^{-1}) = 4500$

Remazeilles & Chluba (2018)

Simulation of correlated μ and T fields

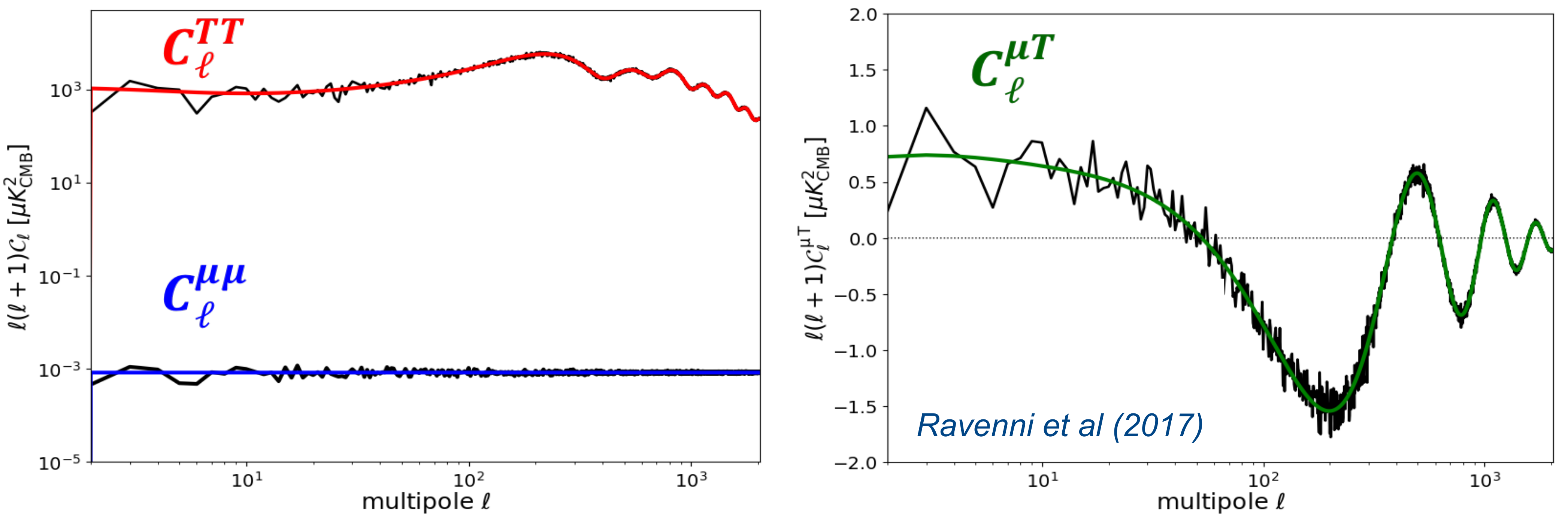

$\langle\mu\rangle = 2\times10^{-8}$ $\qquad f_{NL}(k \simeq 740\ \mathrm{Mpc}^{-1}) = 4500$

Remazeilles & Chluba (2018)

Our full sky simulations

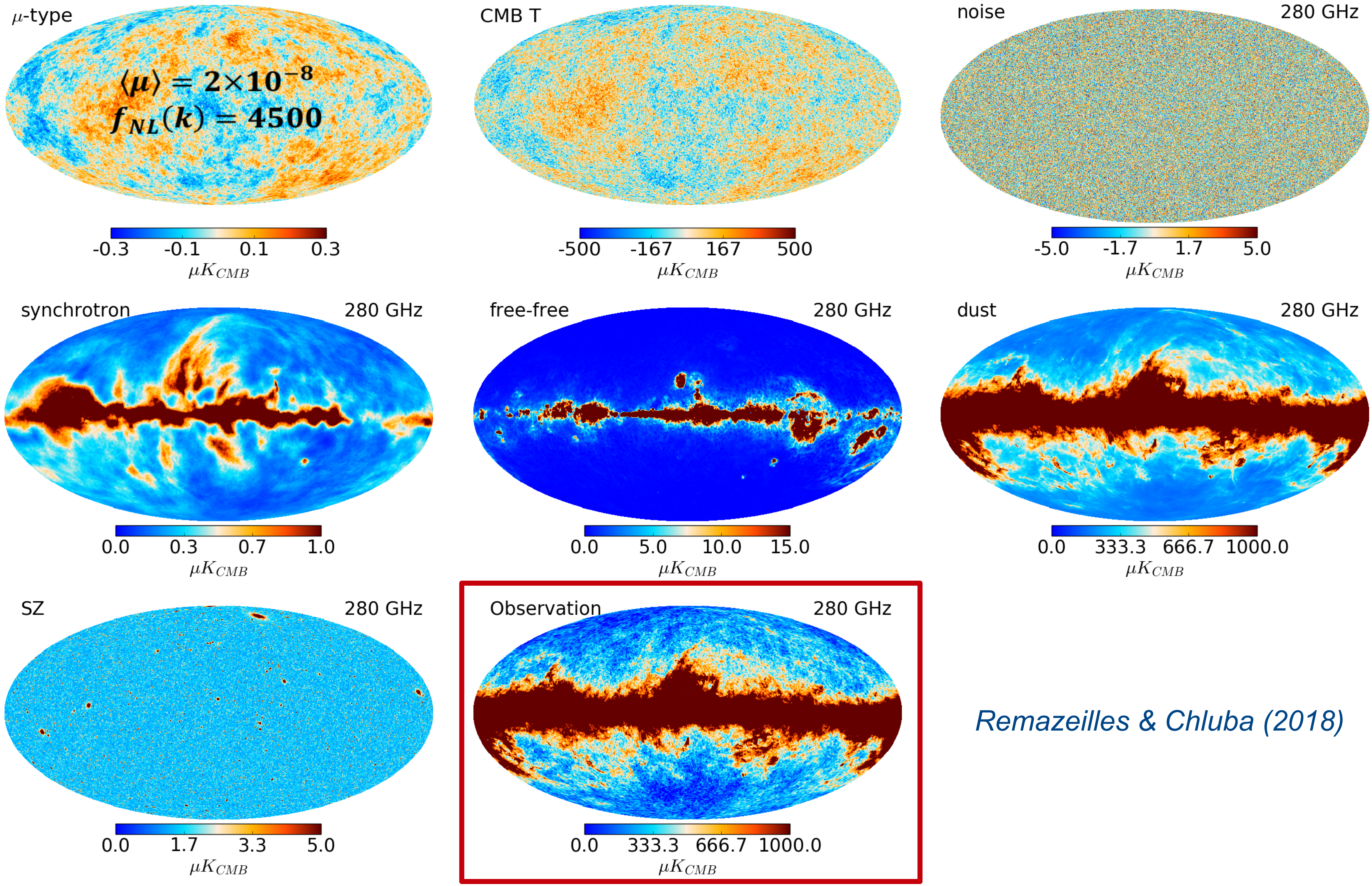

Remazeilles & Chluba (2018)

CMB satellite concepts

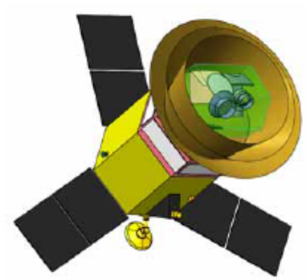

LiteBIRD (JAXA) – Phase A

Suzuki et al, 2018

40 – 402 GHz ; 2.5 μK.arcmin

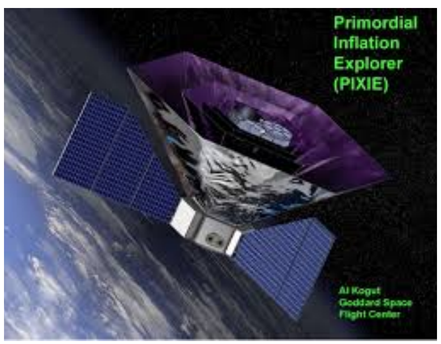

PIXIE (NASA)

Kogut et al., 2011

30 – 6000 GHz ;

6.6 μK.arcmin
(Δν=30 GHz)

CORE (ESA)
CMB-Bharat (ISRO)

Delabrouille et al, 2018

60 – 600 GHz ; 1.7 μK.arcmin

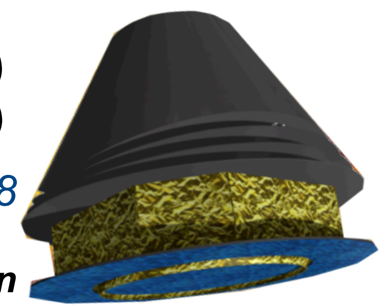

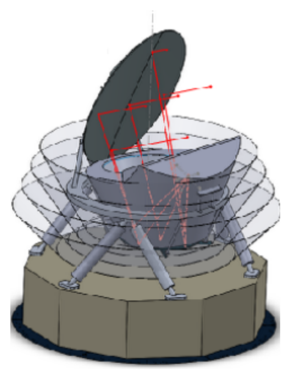

PICO (NASA)
Probe Mission Concept Study 2018

Shaul Hanany, priv. comm.

21 – 800 GHz ; 1.1 μK.arcmin

Constrained-ILC μ-map reconstruction

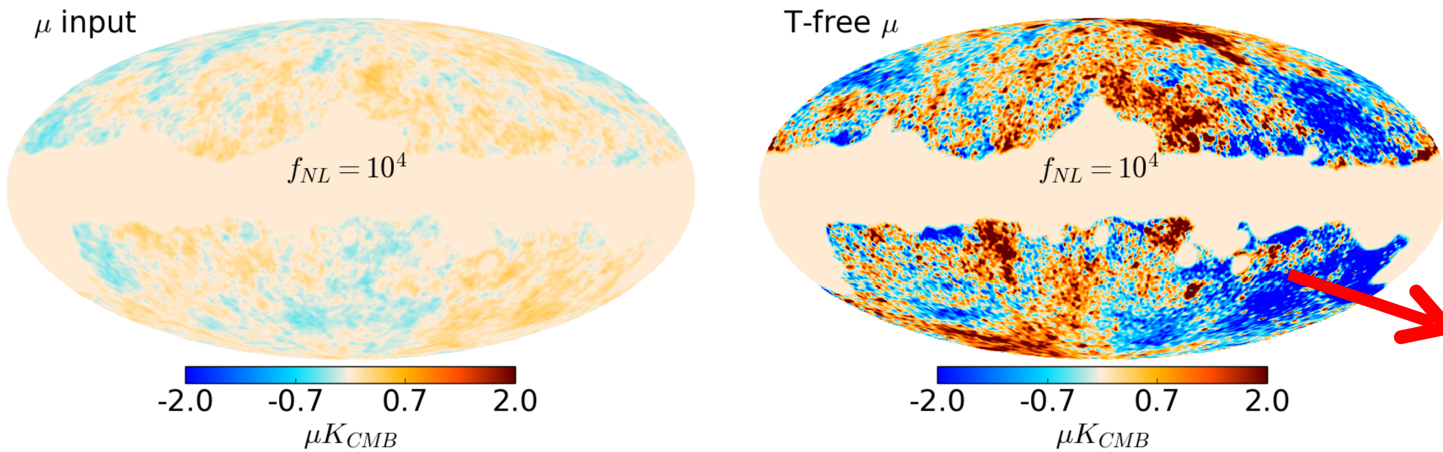

significant foreground contamination

Remazeilles & Chluba (2018)

Constrained-ILC μ-map reconstruction

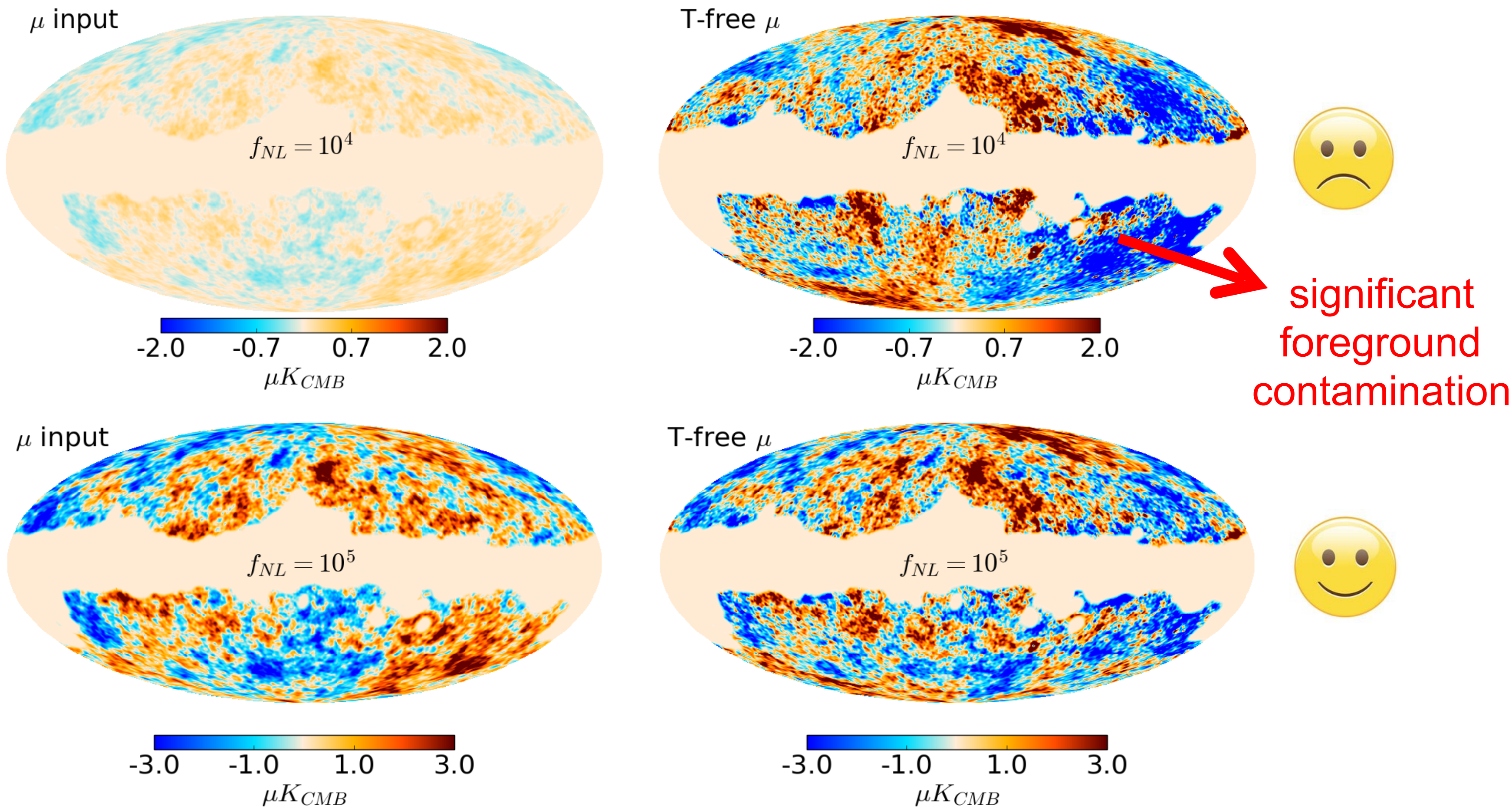

Remazeilles & Chluba (2018)

Constrained-ILC μ-map reconstruction

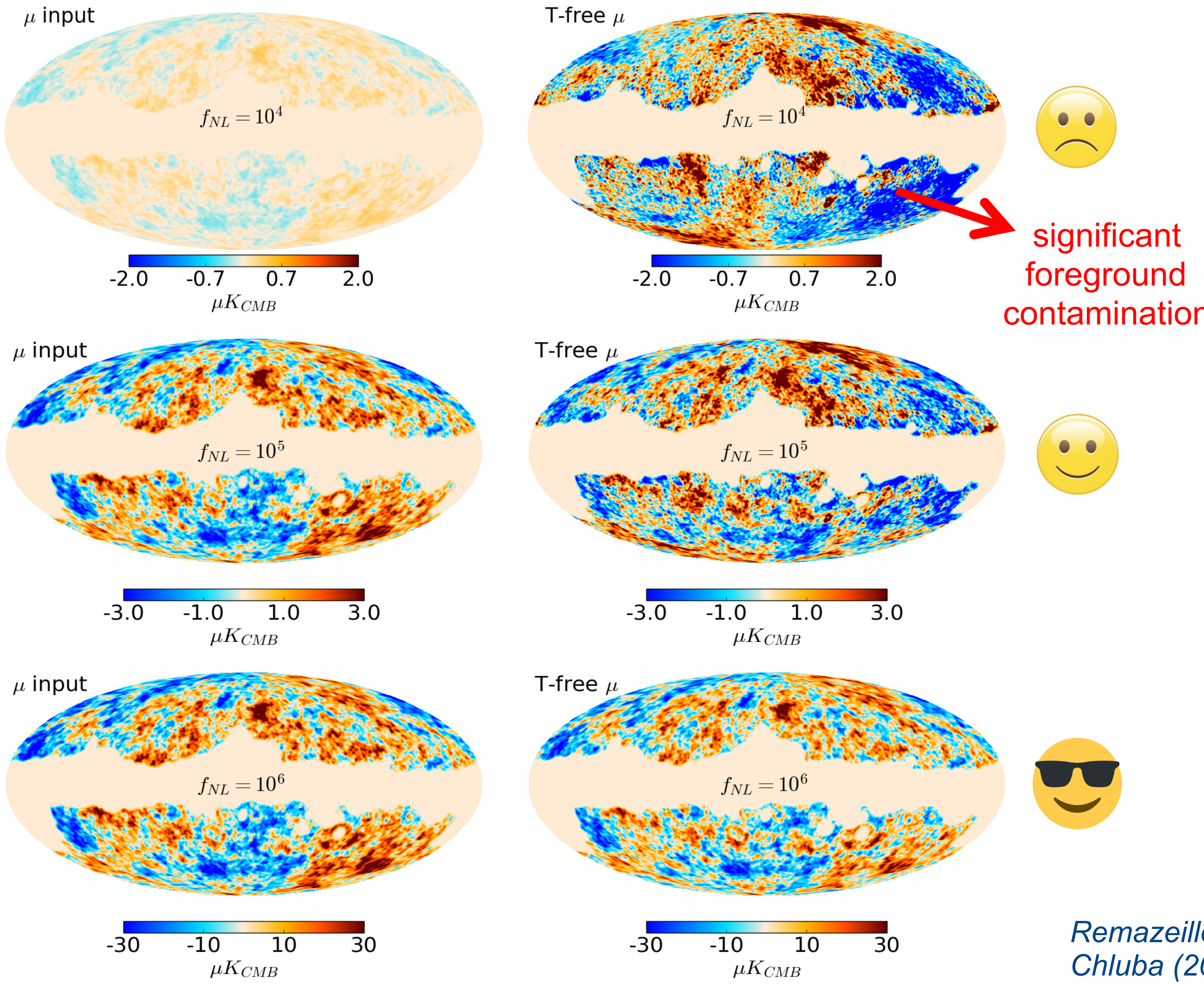

Remazeilles & Chluba (2018)

Constrained-ILC μ-map reconstruction

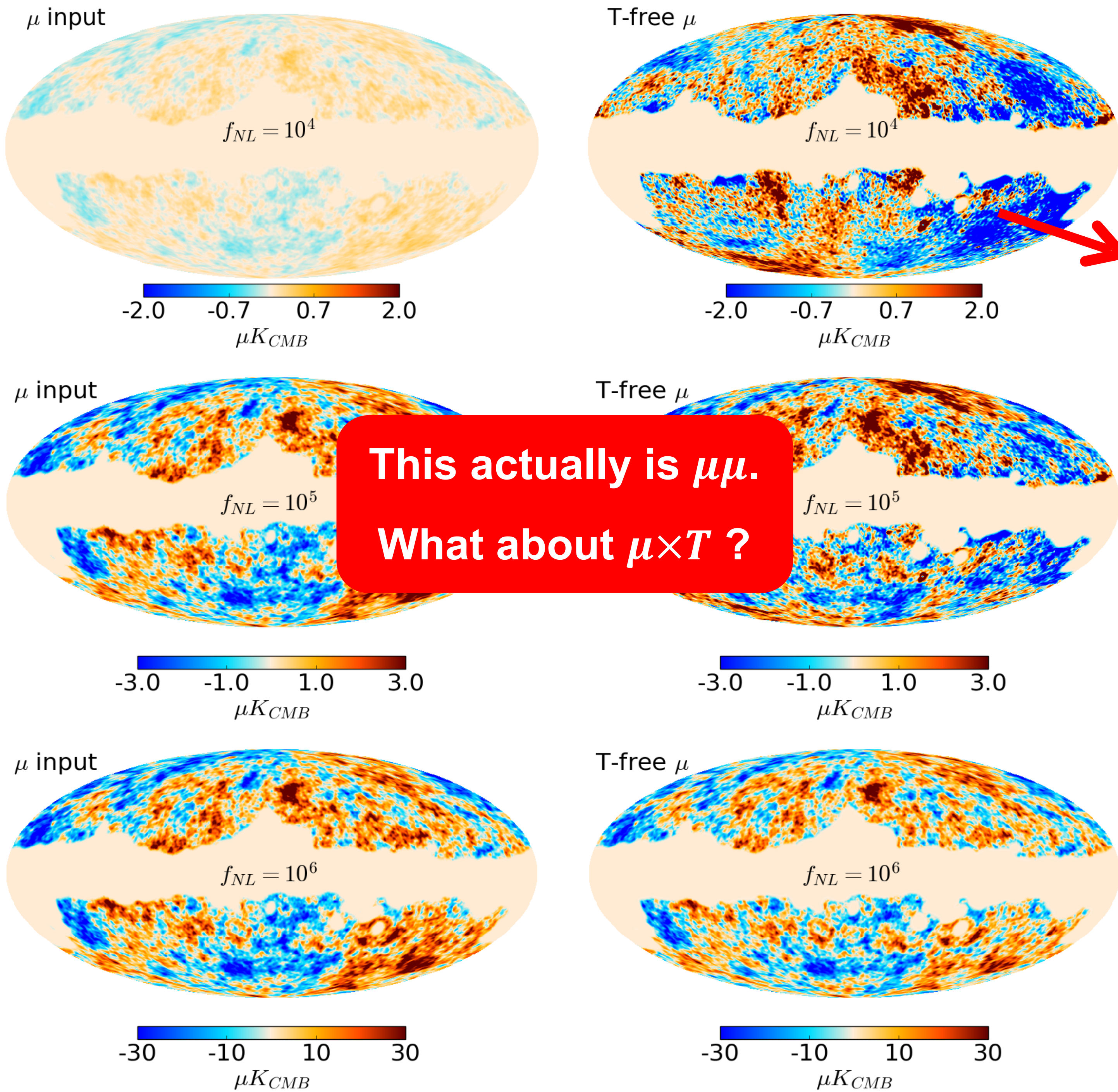

significant foreground contamination

This actually is $\mu\mu$.

What about $\mu{\times}T$?

Remazeilles & Chluba (2018)

$C_\ell^{\mu T}$ reconstruction: $f_{NL} = 4500$ (w/o foregrounds)

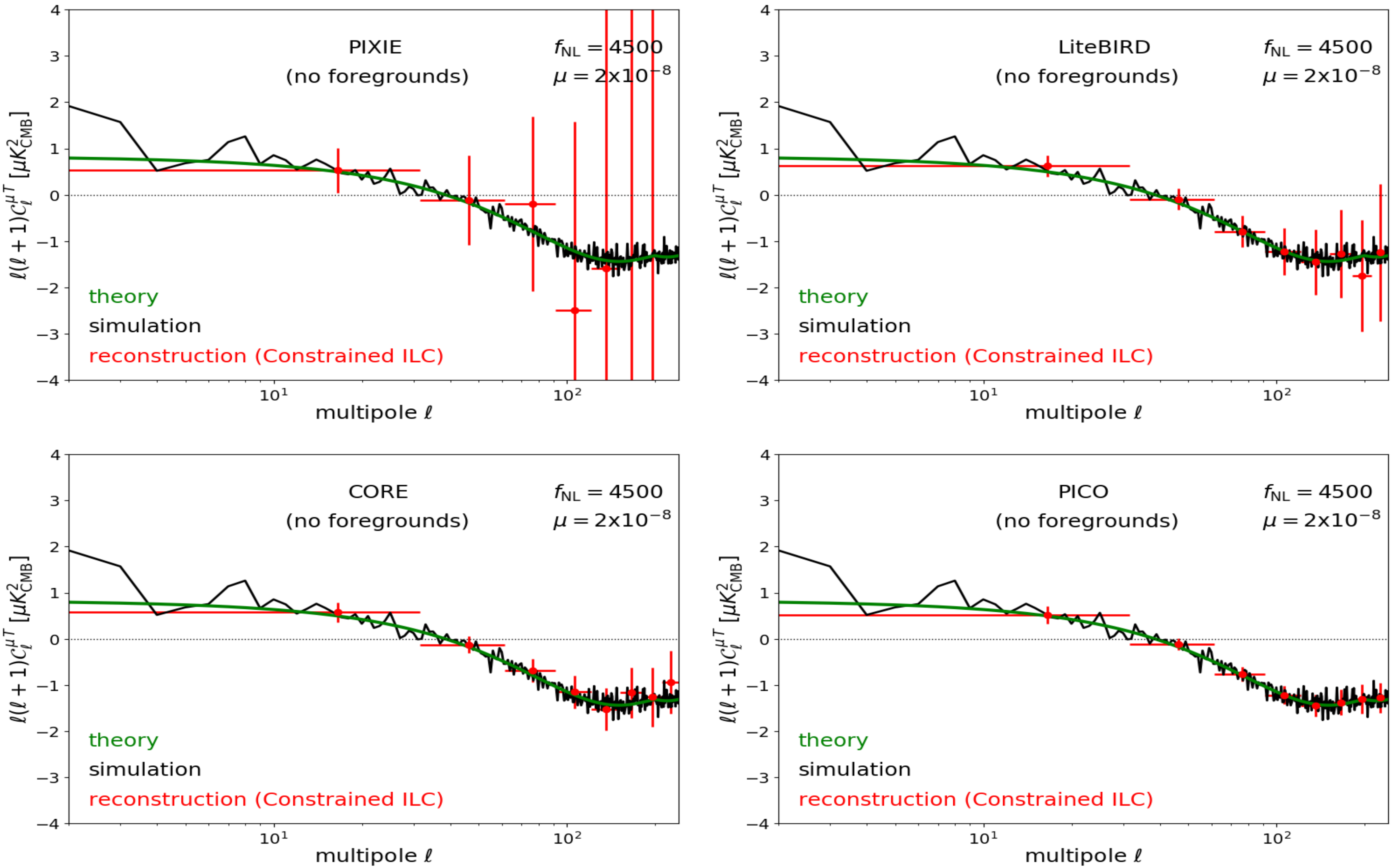

Remazeilles & Chluba (2018)

$C_\ell^{\mu T}$ reconstruction: $f_{NL} = 4500$ (with foregrounds)

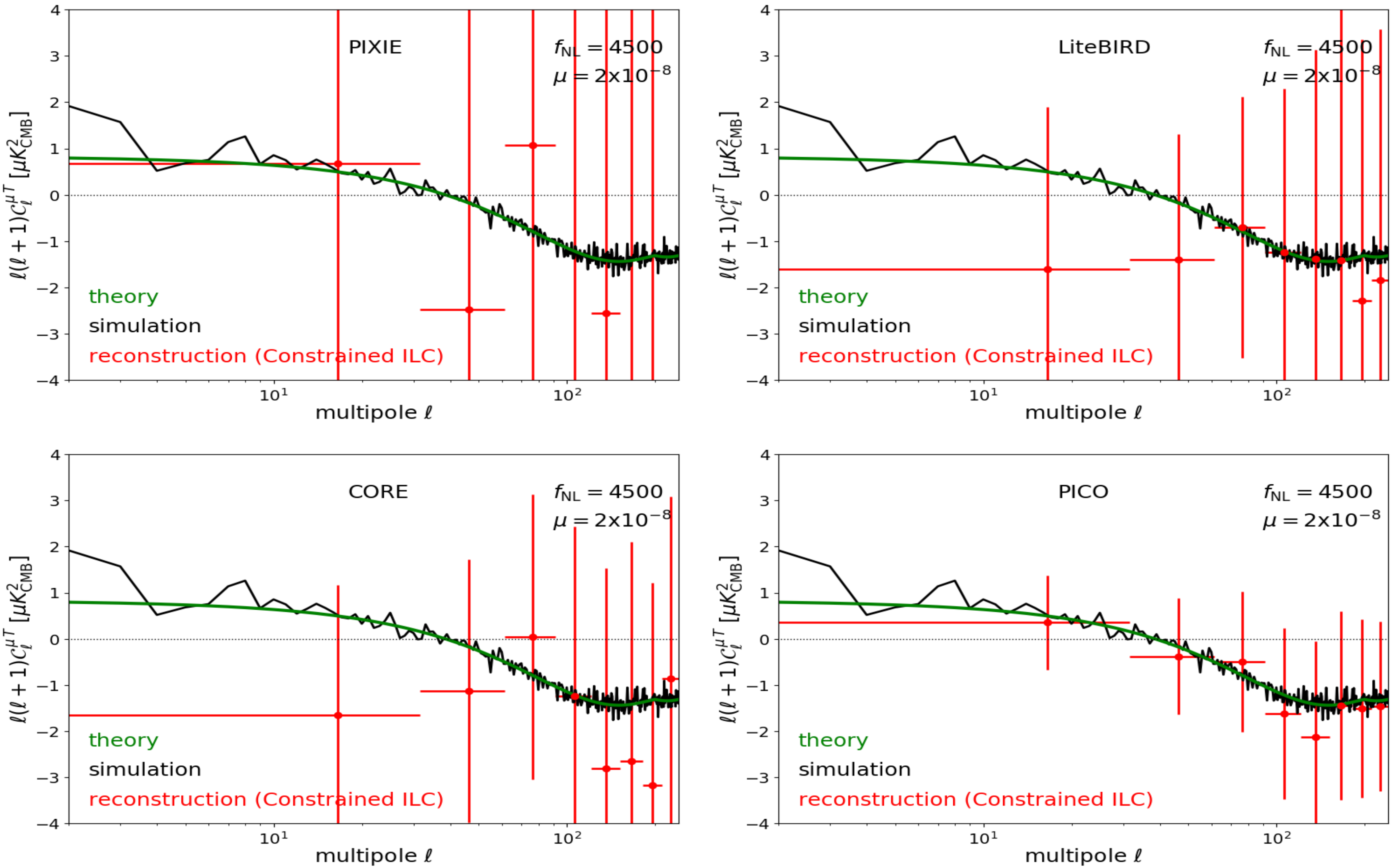

Remazeilles & Chluba (2018)

$C_\ell^{\mu T}$ reconstruction: $f_{NL} = 4500$ (with foregrounds)

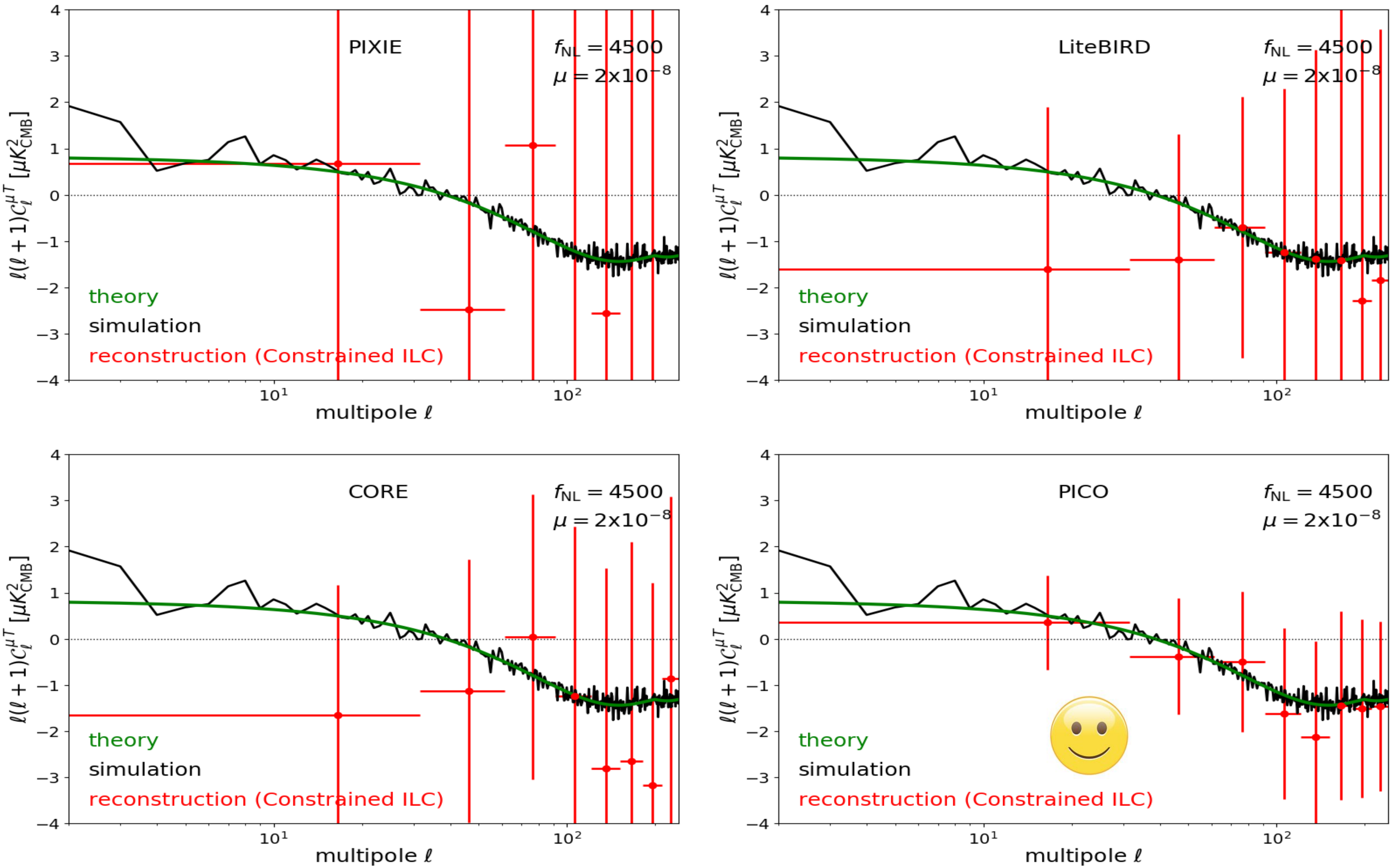

Remazeilles & Chluba (2018)

$C_\ell^{\mu T}$ reconstruction: $f_{NL} = 10^4$ (with foregrounds)

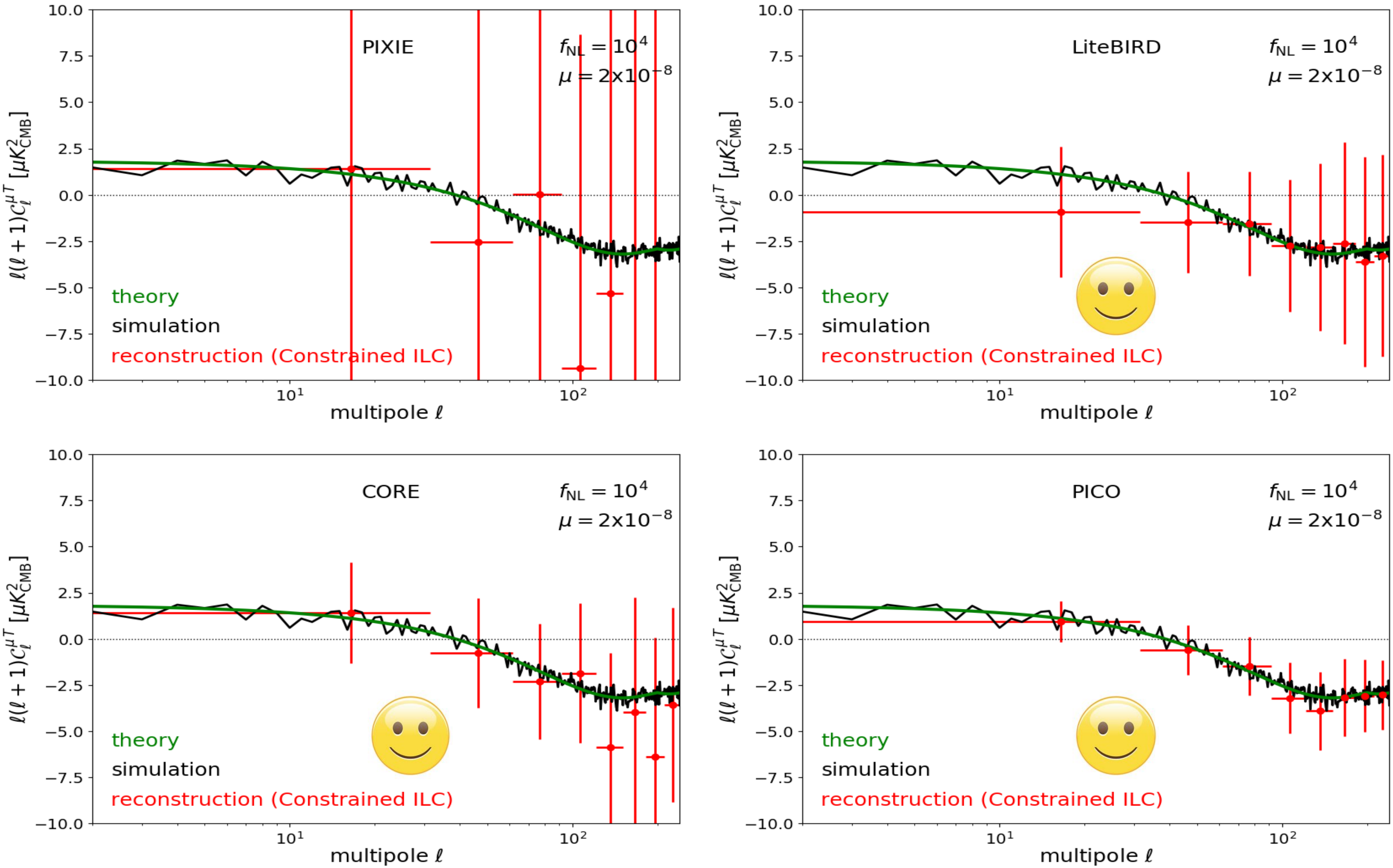

Remazeilles & Chluba (2018)

$C_\ell^{\mu T}$ reconstruction: $f_{NL} = 10^5$ (with foregrounds)

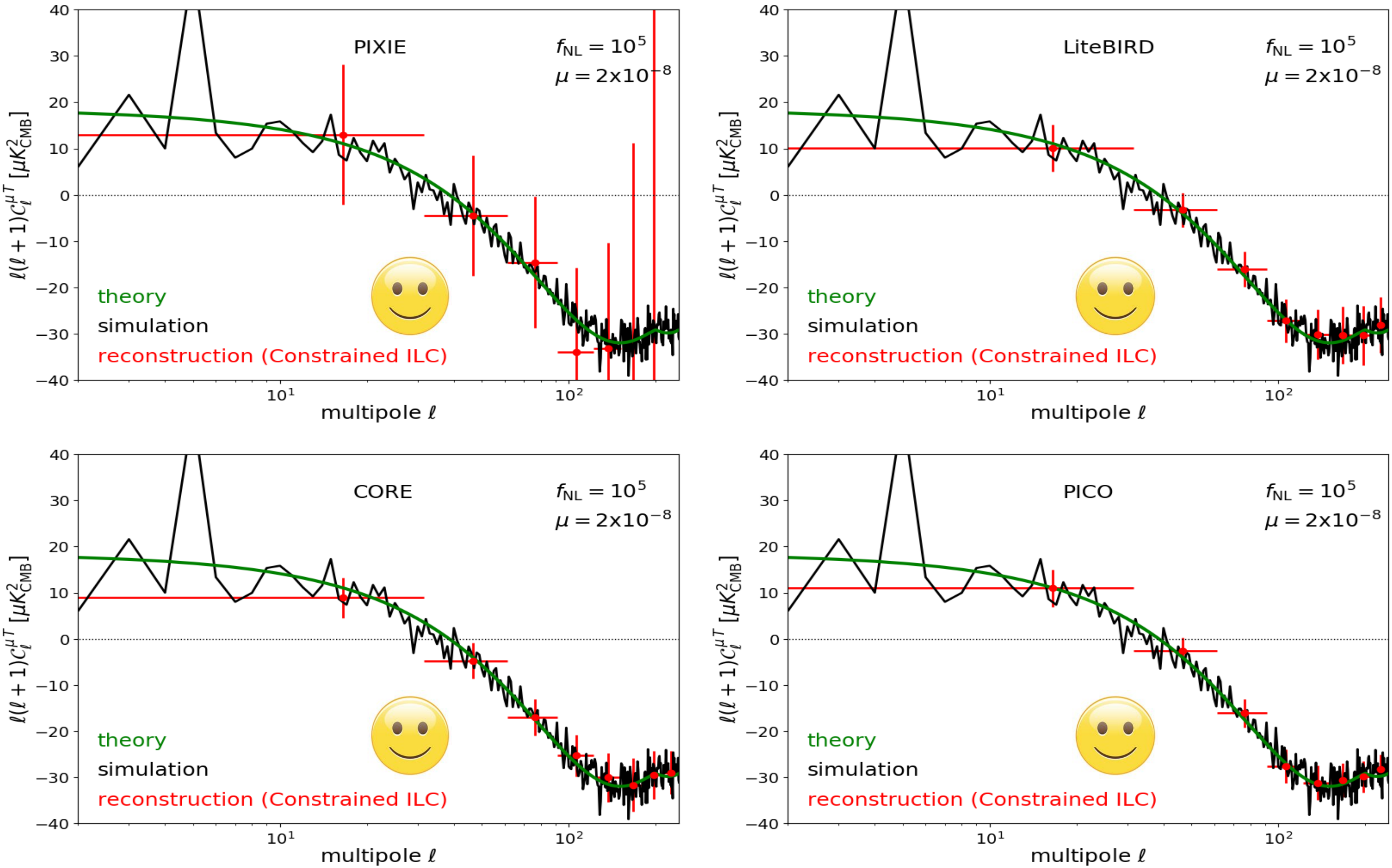

Remazeilles & Chluba (2018)

Forecasts on small-scale non-Gaussianity

Table 5. Detection forecasts on $f_{\rm NL}(k \simeq 740\,{\rm Mpc}^{-1})$ after component separation, based on multipoles $2 \leqslant \ell \leqslant 200$.

$f_{\rm NL}$ (fiducial)	10^5	10^4	4500	4500 w/o foregrounds
PIXIE	$(1.11 \pm 0.40) \times 10^5$	$(2.17 \pm 3.90) \times 10^4$	$(1.5 \pm 3.9) \times 10^4$	4778 ± 3868
	2.5σ	–	–	1.2σ
LiteBIRD	$(0.98 \pm 0.08) \times 10^5$	$(0.91 \pm 0.68) \times 10^4$	4272 ± 6788	4753 ± 930
	12.5σ	1.5σ	–	4.8σ
CORE	$(0.97 \pm 0.08) \times 10^5$	$(1.35 \pm 0.74) \times 10^4$	5692 ± 6397	4336 ± 653
	12.5σ	1.4σ	–	6.9σ
PICO	$(0.99 \pm 0.06) \times 10^5$	$(1.07 \pm 0.30) \times 10^4$	5094 ± 2929	4480 ± 371
	17.8σ	3.3σ	1.5σ	12.1σ

PICO is in the best position to detect the μ-T correlation signal at $f_{NL}(k \simeq 740\ \mathrm{Mpc}^{-1}) \lesssim 4500$ in the presence of foregrounds

Remazeilles & Chluba (2018)

Null-test: μ-T signal reconstruction for $f_{NL} = 0$

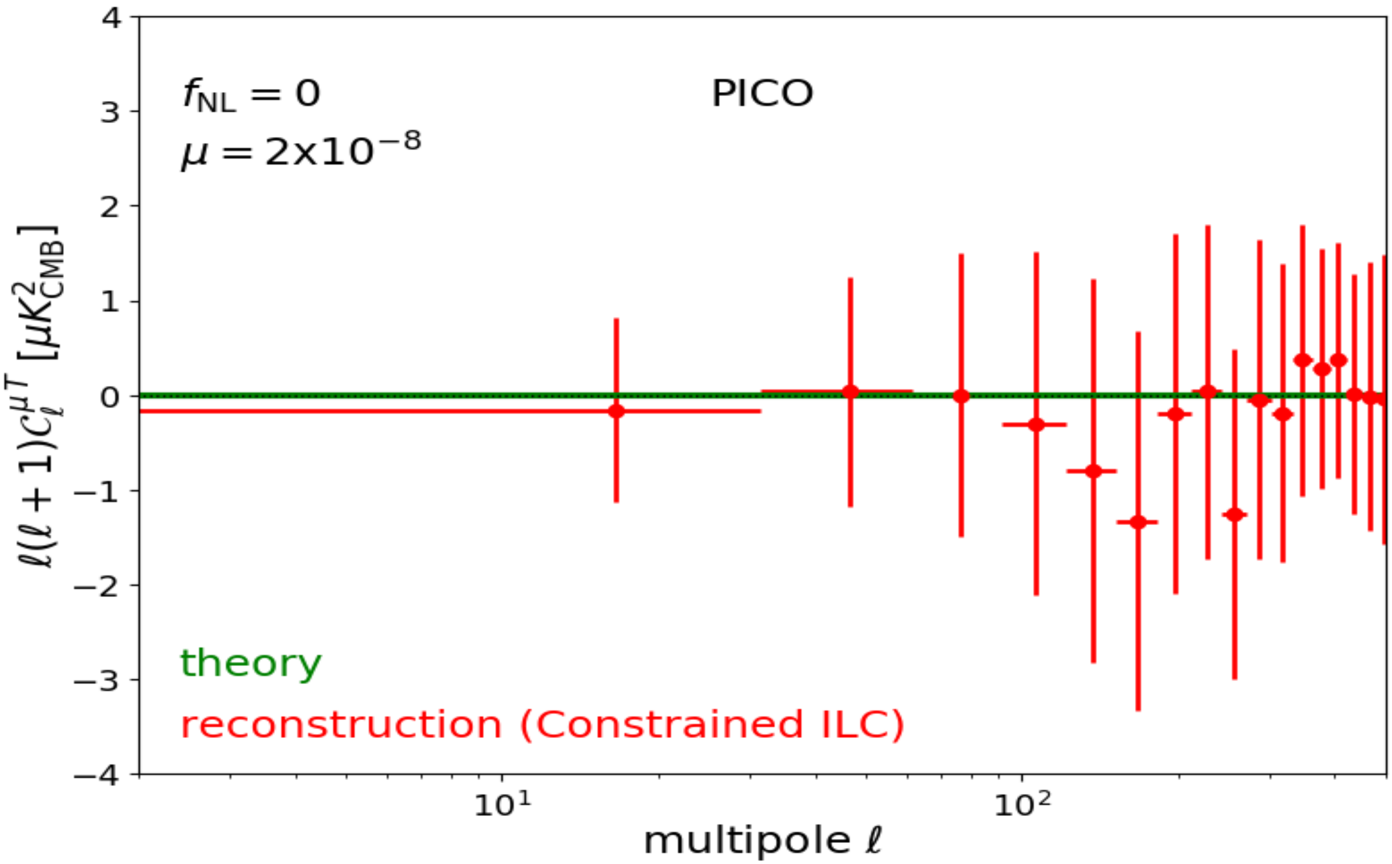

In the absence of μ-distortion anisotropies, the reconstruction by Constrained ILC is consistent with $f_{NL} = 0$

Remazeilles & Chluba (2018)

Minimum detection limit

Table 6. Detection limits for *PICO* on $f_{\rm NL}(k \simeq 740\,{\rm Mpc}^{-1})$ after component separation, based on the multipole range $2 \leqslant \ell \leqslant 500$ using the model of Ravenni et al. (2017) to describe the $\mu - T$ cross-correlation. Foregrounds are included in all cases and the fiducial $f_{\rm NL}$ parameter was varied.

$f_{\rm NL}$ (fiducial)	−4500	0	4500
PICO	-2996 ± 2112 2σ	1325 ± 2114 –	5698 ± 2121 2σ

Minimum detection limit by PICO in the presence of foregrounds:

$$|f_{NL}(k \simeq 740\ \mathrm{Mpc}^{-1}| \gtrsim 2100$$

Remazeilles & Chluba (2018)

More detectors or more frequencies?

"Enhanced LiteBIRD" with $100 \times$ more detectors

0.2 μK. arcmin, 40 - 400 GHz

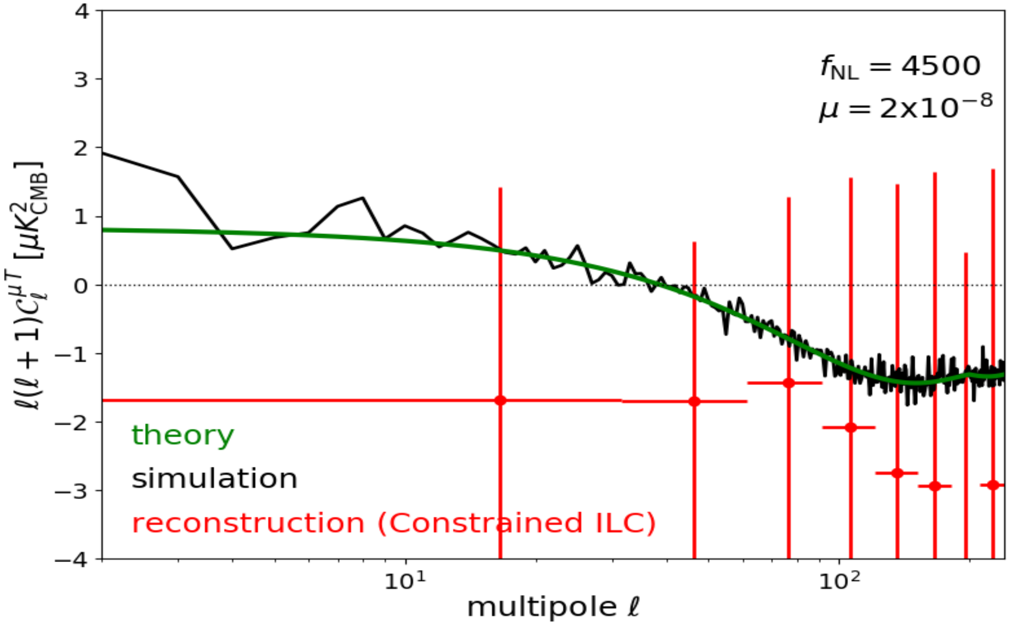

PICO

0.8 μK. arcmin, 20 - 800 GHz

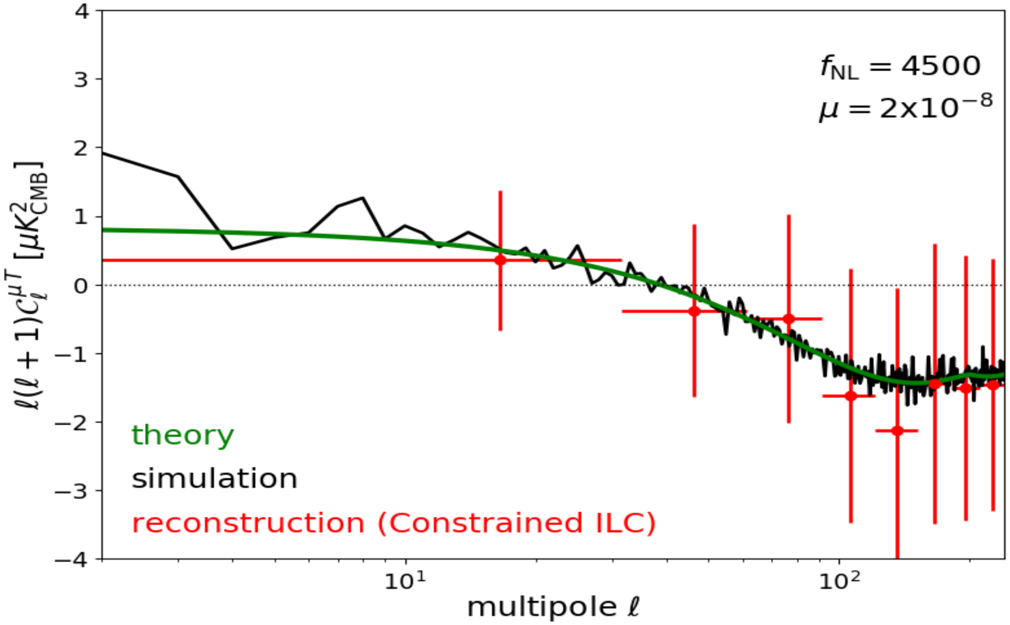

Extended frequency coverage at frequencies $\nu \lesssim 40$ GHz and $\nu \gtrsim 400$ GHz provides more leverage than increased channel sensitivity

Remazeilles & Chluba (2018)

What part of the frequency range matters?

- Discarding PICO frequencies above $\nu > 400$ GHz degrades component separation results by $\simeq 7\%$
- Discarding PICO frequencies below $\nu < 40$ GHz degrades component separation results by $\simeq 30\%$

Low-frequencies $\nu < 40\ GHz$ have more constraining power on μ-distortion anisotropies than high-frequencies $\nu > 400\ GHz$

Remazeilles & Chluba (2018)

→ consistent with the conclusions of *Abitbol et al (2017)* for monopole distortions

Inter-calibration errors kill CMB temperature (so may bias μ-T measurements)

Calibration errors can screw up an ILC in the high signal-to-noise regimes, through partial cancellation of the variance of the CMB temperature anisotropies
Dick, Remazeilles, Delabrouille, MNRAS (2010)

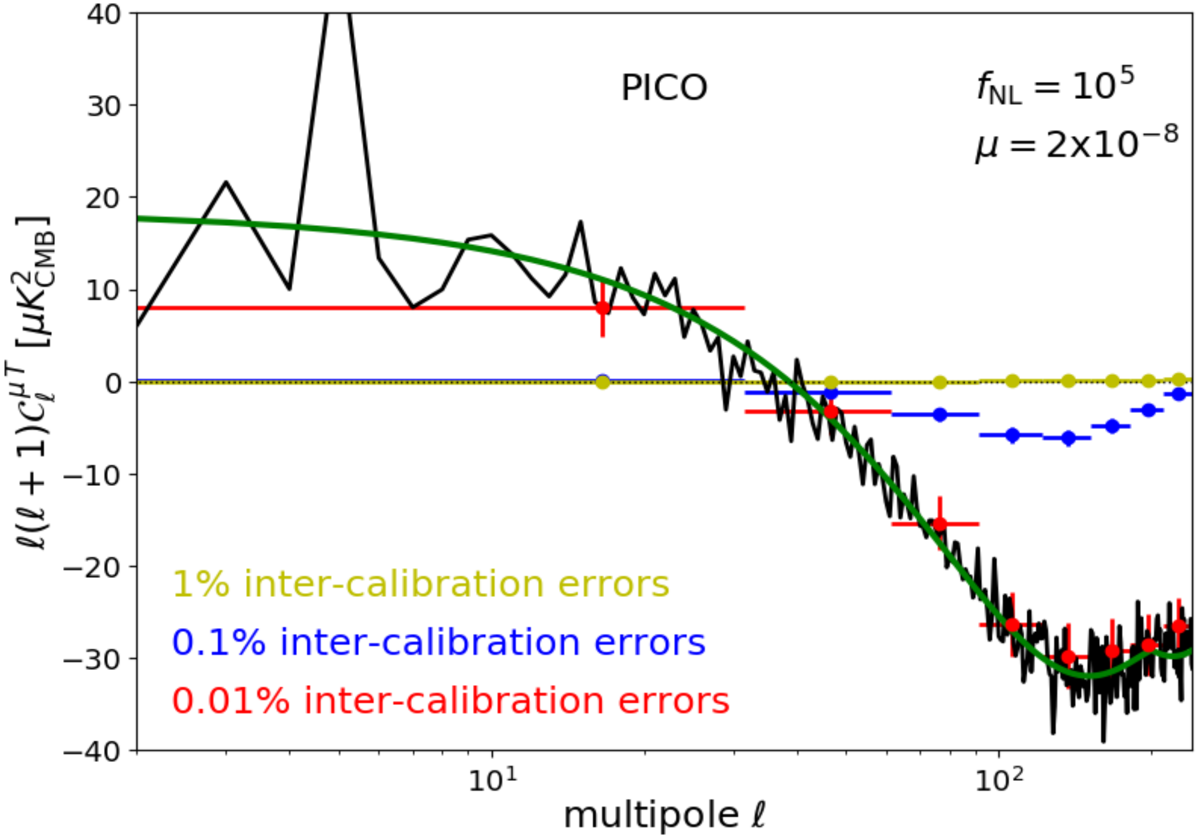

The allowed inter-channel calibration uncertainty for PICO is 0.01 %

(The promise of CORE was to achieve such calibration accuracy)

Remazeilles & Chluba (2018)

Conclusions

Remazeilles & Chluba (2018)

- We have computed the first forecasts on the detection of the μ-T correlation signal and $f_{NL}(k \simeq 740\ \mathrm{Mpc}^{-1})$ in the presence of foregrounds with future CMB satellites
- We have proposed a tricky component separation approach, the "Constrained-ILC", to null out residual CMB TT correlations in the μ-T correlation signal
- Among CMB satellite concepts, PICO is in the best position to detect anisotropic μ-type distortions in the presence of foregrounds, with $f_{NL}(k \simeq 740\ \mathrm{Mpc}^{-1}) \lesssim 2100$
- Optimization: more detectors or more frequencies?

  Extended frequency coverage at frequencies $\nu \lesssim 40\ GHz$ and $\nu \gtrsim 400\ GHz$ provides more leverage than increased channel sensitivity

  Low-frequencies $\nu \lesssim 40\ GHz$ have more constraining power on μ-distortions than high-frequencies $\nu \gtrsim 400\ GHz$

- Spectrometers like PIXIE or PRISTINE still needed for μ-distortion anisotropies to break the $f_{NL}\langle\mu\rangle$ degeneracy

Thank you for your attention!

Backup slides

Averaging effects

dust spectral indices in the sky

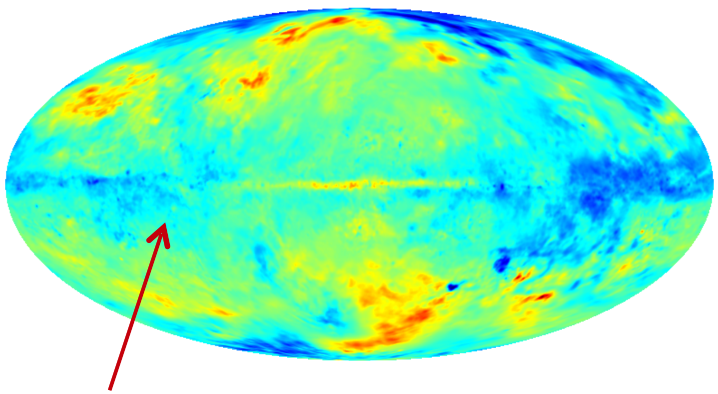

one value β_{dust} per line-of-sight

mapping / pixelization

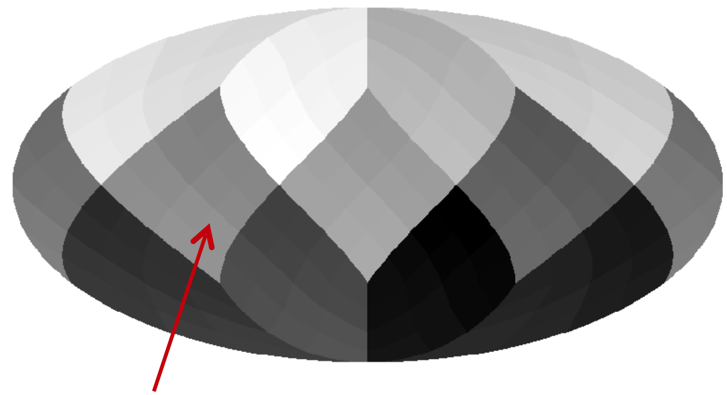

many β_{dust} values per pixel

→ effective SED: $\sum_i \nu^{\beta_i} \neq \nu^{\beta}$

- Because of averaging different line-of-sight SEDs within a pixel/beam, the actual SED of foregrounds *in the maps* differs from the physical SED *in the sky*
  – Chluba et al 2017

- Spurious SED curvatures created by pixel averaging effects, if ignored in the parametric fit, may bias primordial B-modes at the level of $\Delta r \sim 10^{-3}$
  – Remazeilles et al 2017, for the CORE collaboration

- The Constrained-ILC method is blind (no parametrization / assumption on foregrounds), therefore fairly insensitive to averaging effects
  – Remazeilles & Chluba 2018

Importance of spatial resolution

Despite a very broad frequency coverage, PIXIE constraints on anisotropic μ-distortions are of poorer quality than those from LiteBIRD, CORE, PICO

→ *because of lower sensitivity and lower spatial resolution*

- We find that increasing PIXIE resolution from 96' to 40', while keeping its baseline sensitivity, would improve $\sigma(f_{NL})$ by 50%

→ *high-resolution channels enable using more correlated information to improve foreground cleaning*

- Suppose the foreground complexity can be captured by 10 degrees of freedom, then 15-20 frequency bands are enough to subtract foregrounds

→ *In this case, the most sensitive experiments will make a difference in the ILC trade-off of minimizing the balance between foreground and noise contaminations*

- However, if foreground complexity relies on more than 20 degrees of freedom, then the broad frequency range of PIXIE will make a difference with respect to imagers

Remazeilles & Chluba (2018)